Three-dimensional seasonal-mean circulation and hydrography on the eastern Scotian Shelf

Guoqi Han

Biological and Physical Oceanography Section, Fisheries and Oceans Canada, Northwest Atlantic Fisheries Centre, St. John's, NewFoundland, Canada

John W. Loder

Ocean Sciences Division, Fisheries and Oceans Canada, Bedford Institute of Oceanography, Dartmouth, Nova Scotia, Canada

Received 6 May 2002; revised 13 November 2002; accepted 31 December 2002; published 2 May 2003.

[1] A three-dimensional nonlinear finite element model with an advanced turbulence scheme is used in conjunction with historical current, temperature, and salinity observations to describe seasonal-mean circulation and hydrography on the eastern Scotian Shelf (ESS). The model solutions consist of density-, wind-, and boundary-driven currents, and associated elevation, hydrographic, and turbulence fields. The M_2 and K_1 tides are simultaneously computed to include the effects of tidally induced turbulent mixing and bottom friction, and tidal rectification. The circulation is dominated by surface-intensified baroclinic nearshore and shelf-break currents, both directed southwestward with prominent seasonal and alongshelf changes. These currents are primarily associated with the equatorward inflow of relatively fresh water from the Gulf of St. Lawrence and Newfoundland Shelf/Slope. Pronounced and persistent influences of outer-shelf banks, inner-shelf basins, and cross-shelf channels are evident in the circulation fields. In particular, the Sable Gully features a year-round cyclonic partial gyre, with a net onshore flow that is greatest in spring. A relatively strong anticyclonic gyre over Sable/Western Bank contrasts a weak partial gyre over Banquereau Bank. The model solutions are in approximate agreement with observed transports and currents for the primary flow features. *INDEX TERMS:* 4255 Oceanography: General: Numerical modeling; 4512 Oceanography: Physical: Currents; 4536 Oceanography: Physical: Hydrography; 4520 Oceanography: Physical: Eddies and mesoscale processes

Citation: Han, G., and J. W. Loder, Three-dimensional seasonal-mean circulation and hydrography on the eastern Scotian Shelf, *J. Geophys. Res.*, *108*(C5), 3136, doi:10.1029/2002JC001463, 2003.

1. Introduction

[2] Recent modeling studies of the Scotian Shelf and Gulf of St. Lawrence (Figure 1a) have not only demonstrated the value of diagnostic models in providing a coarse quantitative representation of seasonal-mean circulation, but have also indicated model limitations in areas with sparse density data coverage [e.g., *Hannah et al.*, 1996; *Sheng and Thompson*, 1996; *Han et al.*, 1997, 1999]. These limitations may be partly mitigated with more density data and boundary tuning; however, prognostic models with coupled density and momentum equations closed by advanced turbulence schemes are required to provide dynamically consistent hydrodynamic fields and realistic mixing parameters [e.g., *Naimie*, 1996; *Han*, 2000; *Hannah et al.*, 2001]. Here we use a prognostic model in conjunction with historical data sets to provide an improved description and understanding of circulation, hydrography, and mixing over the ESS.

[3] The topography of the ESS (Figure 1b) is characterized by shallow outer banks, deep inner basins, and cross-shelf channels. This complex geometry, together with the confluence of the Gulf of St. Lawrence outflow through Cabot Strait (CS), the Labrador Current extension along the shelf break and the cyclonic Slope Water gyre over the continental slope [e.g., *Loder et al.*, 1998], results in pronounced spatial and temporal structure in the region's circulation pattern on various scales of biological and environmental importance. On the shelf scale, the region has variable inflows of relatively fresh Gulf and subpolar water, and relatively saline offshore Slope Water, as well as their associated physical-chemical properties [e.g., *Houghton et al.*, 1978; *Loder et al.*, 1997; *Smith et al.*, 2001; *Petrie and Yeats*, 2000] and organisms [e.g., *Herman et al.*, 1991; *Frank et al.*, 1996; *Head et al.*, 1999]. On the topographic (bank/basin/channel) scale, the structure and variability of circulation features such as partial gyres and cross-shelf flows can have important implications for the survival and interstock mixing of fish larvae [e.g., *Brander and Hurley*, 1992], zooplankton availability in fish nursery

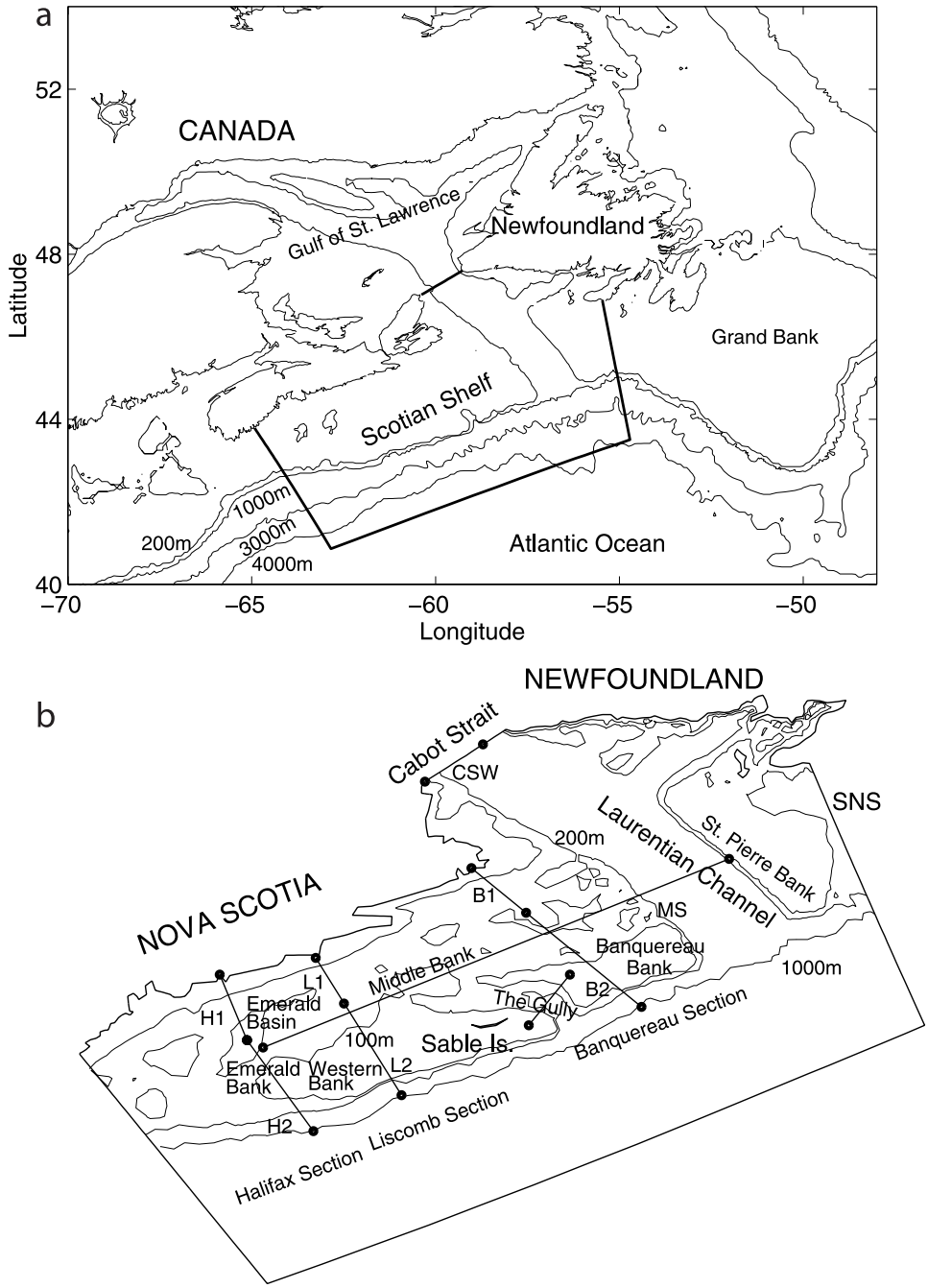

Figure 1. (a) Map showing the eastern Scotian Shelf and adjacent NW Atlantic Ocean. (b) The model domain showing bathymetry and section locations. The Banquereau, Liscomb, and Halifax sections are shown as solid lines, with B1 (B2), L1 (L2), and H1 (H2) indicating their inner (outer) segments. Also displayed are the Cabot Strait West (CSW), midshelf (MS), and Gully sections.

areas [*Taggart et al.*, 1996], nutrient supply to, and organism or pollutant retention in, areas of particular ecological concern such as the Sable Gully [*Harrison and Fenton*, 1998], and the fate of discharges from offshore petroleum production activities [*Gordon et al.*, 2000].

[4] To date, knowledge of the physical oceanography of the ESS has come largely from hydrographic data, mostly from fisheries surveys [e.g., *Page and Losier*, 1994; *Petrie et al.*, 1996], short-term current measurements by the petroleum industry [e.g., *Gregory and Bussard*, 1996], and a few shelf-scale analysis and modeling investigations. This knowledge is limited compared with that from the western and central Scotian Shelf [e.g., *Thompson and Griffin*, 1998; *Hannah et al.*, 2001]. Observational information on the ESS circulation pattern has come from water mass analysis [e.g., *McLellan*, 1954], drift bottle studies

[*Trites and Banks*, 1958], the scattered moored measurements, sea surface slope estimates from altimetry [*Han et al.*, 1993], and the recent diagnostic model studies. In this paper, we use the Dartmouth prognostic finite element model [*Lynch et al.*, 1996; *Naimie*, 1996] to refine initial observationally based hydrographic fields and associated diagnostically computed flow fields for the ESS. The prognostically refined solutions provide observationally based and dynamically consistent three-dimensional (3D) hydrographic, current (seasonal-mean and tidal) and turbulence fields. The primary goals of the study are to provide a quantitative description of seasonal-mean circulation on the ESS with a focus on shelf- and topographic-scale features, and to identify seasonal changes of the circulation and their underlying dynamics.

[5] In section 2, we briefly describe the historical currents data, the circulation model, its initial and boundary conditions, and the solution procedure. Section 3 presents the M_2 and K_1 tidal currents, and section 4 describes and evaluates the seasonal-mean circulation and hydrography. We conclude with a brief summary in section 5.

2. Methodology

2.1. Observational Currents Data

[6] The primary observational data set on ESS currents is a database of moored current measurements from various sources, maintained at the Bedford Institute of Oceanography [*Gregory and Bussard*, 1996]. Monthly mean currents were derived from this database, for months with a minimum of 15 days of data. Typically, each mooring site has observations from one to three depths in 1 or 2 years. For overall comparisons with the model flow fields, seasonal-mean currents and standard deviations (of the monthly about the seasonal means) were computed for each 3D position with at least two monthly means, by averaging over all months and years in each bimonthly season (see below). Model horizontal velocities were linearly interpolated for each position. A number of overall statistics for the observational sites was computed for each seasonal-mean flow field, including the means and standard deviations for each of the observed current speed, the model current speed, the magnitude of the vector velocity difference between the observed and model velocities, and the difference angle between the observed and model velocities. The primary goodness-of-fit index was taken to be a difference ratio defined as the ratio of the sum of the squared magnitudes of the vector velocity differences to the sum of the squared magnitudes of the observed velocities, with lower values indicating better agreement.

[7] Harmonic analyses, in which seven major tidal constituents were simultaneously estimated from various 30-day periods of the archived current meter time series, were carried out for comparison with the model tidal currents.

2.2. Prognostic Model and Mesh

[8] The primary model is the prognostic finite element model QUODDY4 [*Lynch et al.*, 1996; *Naimie*, 1996]. It has 3D nonlinear primitive equations with Boussinesq and hydrostatic approximations, and a level-2.5 turbulence closure scheme [*Mellor and Yamada*, 1982; *Blumberg et al.*, 1992]. The vertical eddy viscosity for momentum, and vertical diffusivity for temperature, salinity and turbulent kinetic energy, and mixing length scale were given a minimum value of 0.0001 m^2/s. The advantage of the prognostic model over a diagnostic approach is the improved dynamic consistency among hydrography, circulation, and turbulence [e.g., *Hannah et al.*, 2001].

[9] The model's fixed horizontal mesh (Figure 2) was derived from *Han et al.*'s [1997] triangular mesh (ss2) by truncating the latter across the western Scotian Shelf (WSS) and increasing its resolution. The resulting mesh (ss3) has 7208 variably spaced nodes and covers the southern Newfoundland Shelf (SNS) and eastern and central Scotian Shelf, with high resolution in shallow areas and those with small topographic length scale ($h/|\nabla h|$, where h is the local water depth). Typical node spacing is 5 km over the shelf. The mesh has open boundaries across CS, the SNS and the WSS, and extends offshore about 200 km beyond the shelf break. The vertical mesh has 21 variably spaced nodes with minimum spacing of 1 m near the sea surface and seabed, and adjusts to track the movement of the sea surface during the model simulations. The model uses realistic topography (from a database with about 7-km resolution) shoreward of the 1000-m isobath, and a false bottom which slopes gently from the 1000-m isobath to 1200 m at the offshore boundary.

2.3. Initial Conditions

[10] Climatological seasonal-mean temperature, salinity and density fields for each of four seasons (nominally January–February, April–May, July–August, and October–November representing winter, spring, summer, and fall, respectively) were taken from previous studies [*Loder et al.*, 1997; *Hannah et al.*, 2001]. These fields were estimated from the Bedford Institute's historical hydrographic database using a four-dimensional optimal linear interpolation procedure. The horizontal grid points were the nodes of the ss2 mesh, the vertical grid points were fixed depths (at intervals of 10 m for 0–60 m, 25 m for 75–250 m, 50 m for 300–500 m, and 100 m for 600–1200 m), and the temporal grid points were the seasonal midtimes. The various ss2 fields were interpolated onto the ss3 mesh to provide initial observationally based hydrographic conditions for the prognostic model solutions.

[11] The initial sea surface elevation and 3D velocity fields for the prognostic models were taken from the seasonal-mean and tidal solutions of the linear diagnostic model FUNDY5 [*Naimie and Lynch*, 1993]. The tidal solutions were forced by elevations at the open boundaries, derived from *de Margerie and Lank* [1986] and *Han et al.* [1996]. The initial seasonal-mean solutions were obtained by specifying baroclinic pressure gradients throughout the model domain, spatially uniform wind stresses at the sea surface, elevations at the SNS and offshore boundaries, and depth-integrated normal velocities on the CS boundary. The baroclinic pressure gradients were derived from the climatological density fields. The seasonal-mean wind stresses were specified using observational estimates (see Figure 2) computed from hourly wind measurements at Sable Island. The SNS and offshore boundary conditions were steric heights derived from the climatological density fields to provide zero sea-bottom flow normal to the boundary. The CS boundary conditions were the depth-integrated velocities associated with zero normal bottom flow, also derived

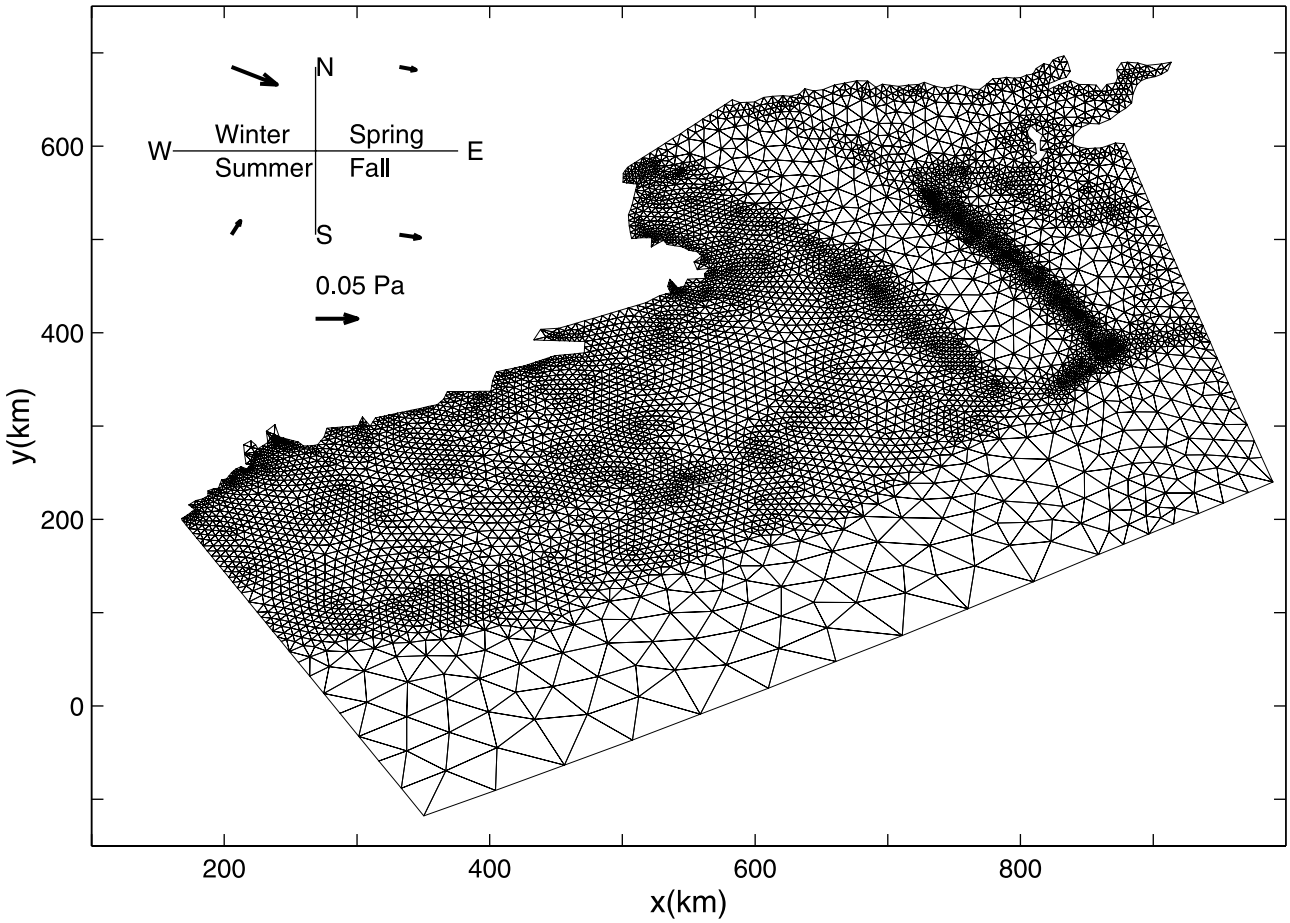

Figure 2. The horizontal finite element grid (ss3) used in the numerical model. The model origin is at 42°N, 67°W. Also shown are the magnitude and direction of the climatological seasonal-mean wind stresses at Sable Island (thick arrows).

from steric computations on the climatological density fields. A geostrophic balance was enforced at the downstream WSS boundary.

2.4. Boundary Conditions on Prognostic Solutions

[12] In the prognostic refinement solutions, temperature and salinity at the open boundaries were fixed to be the climatological values estimated from observations. Zero normal gradients of temperature and salinity were enforced at the lateral land boundaries. Surface temperature was restored toward the initial field on a timescale of half a day (approximately one M_2 cycle), and no-flux conditions were used for salinity and turbulence quantities at the sea surface. At the sea bottom, the turbulent mixing length scale was set to 0.4 m and the turbulent kinetic energy was specified based on the bottom friction velocity.

[13] Elevations were specified along the open boundaries, derived from the appropriate diagnostic solutions described in section 2.3. Zero normal velocity was specified at the land boundaries, and the climatological seasonal wind stresses (Figure 2) were again specified.

2.5. Solution Procedure

[14] The model was integrated forward in time from the initial states using the boundary conditions described in the preceding subsection. The time step was 43.66 s, so there were 1024 time steps in each M_2 tidal cycle. Model solutions were obtained for two cases: one with the temperature and salinity fields at subsurface interior nodes "nudged" toward their initial values on a half-day timescale (like that for the surface temperature field), and the other without any nudging at subsurface nodes.

[15] As noted in the section 1, one of our objectives is to obtain realistic and dynamically self-consistent seasonal-mean and tidal current fields over the ESS. We have thus run the prognostic model, initialized with the observed climatological hydrographic states and associated velocity and elevation fields, with a strategy of sufficient refinement through nudging to reach a quasi-steady dynamical equilibrium among the prognostic variables (temperature, salinity, density, elevation, velocity, and turbulence quantities). The case with subsurface nudging, which is a common practice in numerical modeling of ocean circulation [e.g., *Foreman et al.*, 2000], was included in order to prevent the (nonlinear) prognostic model solution from drifting significantly away from the specified observationally based state (the diagnostic solution). The restoration timescale of half a day was chosen to provide moderate-to-strong nudging, although this may partially suppress tidal evolution of the hydrographic fields (including baroclinic tides). The

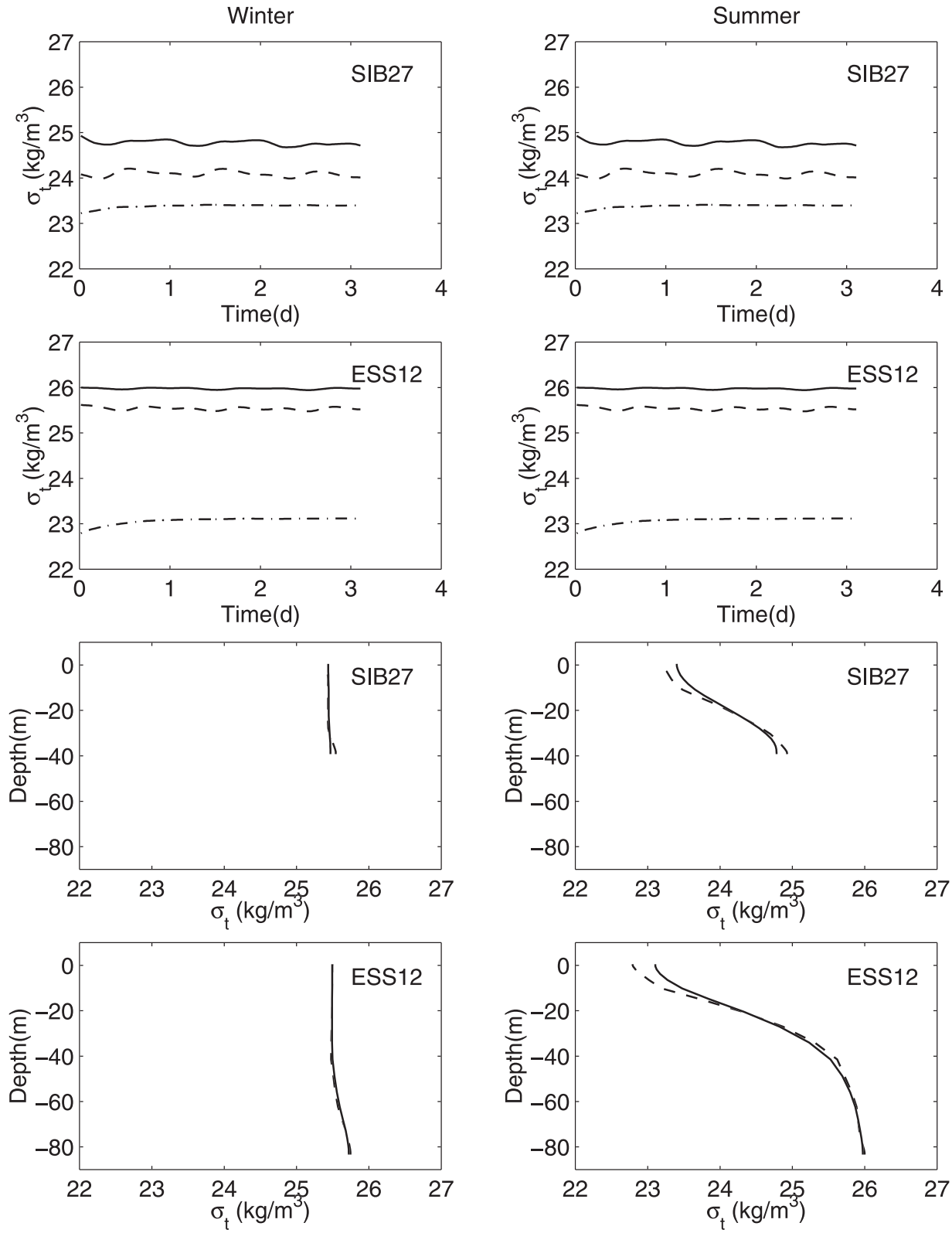

Figure 3. Computed density for representative sites and seasons. Time series (upper four panels) at the surface, middepth, and bottom are shown in dash-dotted, dashed, and solid lines, respectively. Vertical profiles (lower four panels) from the baseline solution and the initial state are shown in solid and dashed lines. Site locations are indicated in Figure 4d.

Table 1. Statistics (Means and Standard Deviations) From the Comparison Between Observed and Model Seasonal-Mean Currents on the Offshore Banks[a]

		Average Speed, cm/s			Velocity Deviations	
Bimonthly Period	No. Obs	Obs	Model	DR	VVD, cm/s	DA, deg
Jan.–Feb.	25	7.2 ± 5.0	6.9 ± 5.9	0.49	4.9 ± 3.7	37 ± 38
Cycles 5 and 6	25	7.2 ± 5.0	9.7 ± 7.9	0.83	6.0 ± 5.3	29 ± 33
Diagnostic	25	7.2 ± 5.0	4.5 ± 3.4	0.99	7.0 ± 5.2	73 ± 68
April–May	23	6.9 ± 4.5	10.2 ± 10.3	2.10	10.1 ± 6.5	87 ± 63
July–Aug.	17	4.6 ± 3.2	9.1 ± 5.3	2.16	7.1 ± 4.1	71 ± 77
Oct.–Nov.	13	5.2 ± 4.4	6.2 ± 5.6	0.78	4.9 ± 3.5	53 ± 40
Cycles 5 and 6	13	5.2 ± 4.4	6.4 ± 3.6	0.54	4.5 ± 2.2	50 ± 36
Diagnostic	13	5.2 ± 4.4	5.1 ± 5.7	0.78	4.8 ± 3.7	72 ± 62

[a]The model currents are from the baseline solutions (cycles 3–4) for the four seasons, and also cycles 5 and 6 and initial conditions (diagnostic) of the winter and fall solutions. The difference ratio (DR) is defined as the ratio of the sum of squared differences between the observed and modeled velocities to the sum of squared observed currents. The vector velocity difference (VVD, cm/s) is the magnitude of the difference vector between the observed and modeled velocities. The difference angle (DA, degrees) is the magnitude of their difference in direction.

approach in essence is a local dynamical fit to the observational data, with the prognostic variables constrained at the open boundaries, but allowed to evolve in the interior.

[16] During the first couple of M_2 tidal cycles, the model solutions showed a rapid adjustment dominated by the development of a bottom boundary layer. Without the subsurface nudging, the best agreement of the model solution with observed currents occurred during M_2 tidal cycles 2–3, but the solutions diverge significantly from reality afterward. With the subsurface nudging, the model was run for eight M_2 tidal cycles (about 4 days), and the model output for cycles 3–4, 5–6, and 7–8 was used in harmonic analyses to retrieve the seasonal-mean and tidal components for various stages of prognostic refinement.

[17] The seasonal-mean and tidal currents from M_2 cycles 3 and 4 with subsurface nudging have been chosen as baseline solutions. This choice is based on the degree of temperature and salinity adjustment arising from local tidal mixing, and the comparison with observed seasonal-mean currents. The initial local hydrographic adjustment has largely been completed after the first two cycles (Figure 3, upper four panels). At the end of cycle 4, the establishment of a well-mixed bottom boundary layer is evident, e.g., at SIB27 in summer (although it may be too thin in some seasons), and the model dynamics have also eliminated any vertical instability existing in the initial density distribution, e.g., at ESS12 in winter (Figure 3, lower four panels). The model-observation current statistics generally show best agreement for cycles 3–4 and 5–6 (Tables 1 and 2), although the agreement is poor in spring and summer (see later).

3. Tidal Currents

[18] Background on the major semidiurnal and diurnal tidal elevations and currents on the ESS can be found in the work of *Moody et al.* [1984], *de Margerie and Lank* [1986], and *Han et al.* [1996]. The principal reason for including the M_2 and K_1 constituents in the present study is to provide realistic estimates of turbulent mixing for the seasonal-mean fields. Therefore we only briefly discuss the model tidal currents with an emphasis on their spatial structure and mixing effects.

3.1. The M_2 Tide

[19] The model M_2 tidal elevations (not shown) are nearly in phase over the entire ESS, with lags increasing by less than 5° from the Banquereau to Halifax sections (Figure 1b). This is consistent with the M_2 tidal wave approaching the ESS, and subsequently, the Nova Scotia coast nearly perpendicularly from the deep ocean. The model elevation amplitude is about 50 cm increasing shoreward and westward, consistent with observations [e.g., *Moody et al.*, 1984].

[20] Computed M_2 tidal currents (illustrated by the spring solution in Figure 4a) reflect the influences of topography on current magnitude, with a significant contrast between the inner shelf and shallow outer banks. The amplitudes are about 5 cm/s or less over the inner shelf, while those over the outer shelf can exceed 30 cm/s. The strongest currents occur just west and east of Sable Island, with slightly lower peak currents over Banquereau and Middle Banks. The current ellipses are generally elongated in the cross-shelf direction, with an eccentricity of about 0.7 over the outer banks consistent with continuity and rotational effects in shallow water at midlatitude.

[21] The M_2 tidal currents at two current mooring sites in the winter and summer model solutions are compared with observational estimates from the 30-day tidal analyses in Figure 5. Overall, there is good agreement between the model solutions and the moored measurements, but there are significant discrepancies at some depths in the two sites. The observational estimates have substantial temporal variability that exceeds the winter-summer model differences in some cases. At SIB27, the summer solutions agree better with the observational current structure in the vertical than the winter solutions.

3.2. The K_1 Tide

[22] The computed K_1 tide (not shown) has elevation amplitudes under 10 cm over the entire ESS, and an

Table 2. Statistics (Means and Standard Deviations) From the Comparison Between Observed and Modeled (the Baseline Solution and the Solution From Cycles 5 and 6 in Winter) Mean Currents Over the Inner Scotian Shelf[a]

Solution		Average Speed, cm/s			Velocity Deviations	
Cycles	No. Obs	Obs	Model	DR	VVD, cm/s	DA, deg
3–4	18	12.4 ± 7.3	13.2 ± 5.9	0.13	4.7 ± 2.3	6 ± 5
5–6	18	12.4 ± 7.3	10.8 ± 5.7	0.14	4.7 ± 2.4	13 ± 13

[a]See Table 1 for definitions.

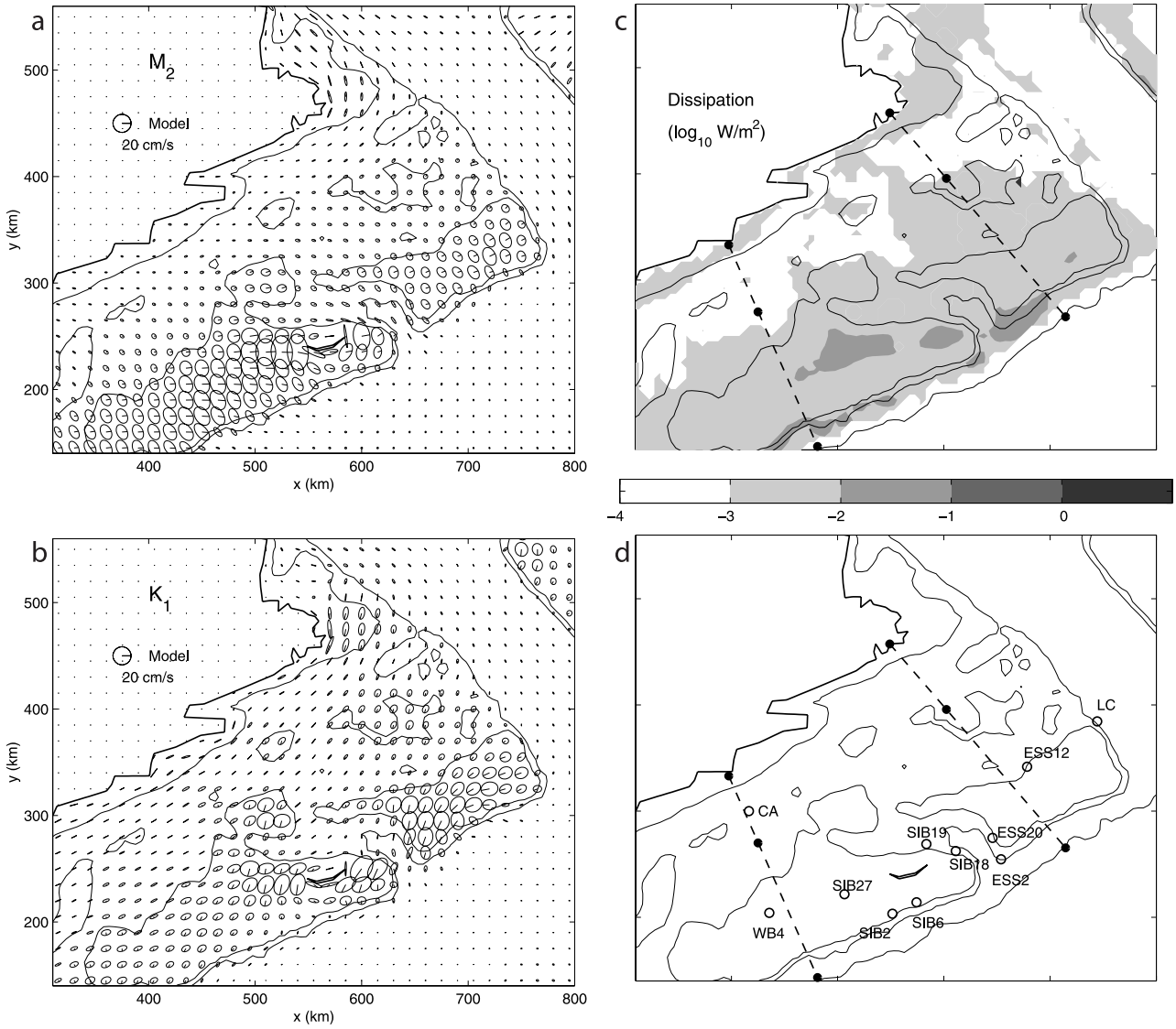

Figure 4. (a) Model M_2 tidal current ellipses (depth-averaged) in spring. (b) Same as Figure 4a, but for K_1. (c) Depth-integrated dissipation rate (W/m^2) in the spring solution. (d) Locations of selected observational sites. The model results in Figures 4a and 4b are subsampled for clarity of presentation.

amphidromic point in Laurentian Channel between the ESS and SNS. The location of the latter is consistent with *Han et al.*'s [1996] findings from satellite altimetry, but is different from previous suggestions of its location near Sable Island [e.g., *Moody et al.*, 1984].

[23] Model K_1 currents over the inner shelf (illustrated by the spring solution in Figure 4b), are rectilinear in the along-shelf direction, with their magnitudes slightly greater than those of the M_2 currents. Over the outer banks the current ellipses remain oriented in the along-shelf direction, but are more circular than on the inner shelf. The current magnitudes are again amplified (up to 20 cm/s) over the banks, especially over western Banquereau Bank and near Sable Island. The general intensification of the K_1 currents is much stronger than expected from Kelvin wave theory, and may be explained by the occurrence of a resonant first-mode shelf wave at the K_1 frequency [*Han*, 2000]. The intensification is expected to be strongly dependent on the bottom topography (and also possibly on stratification), so high resolution of the topography is expected to be crucial in obtaining accurate currents.

[24] Comparisons of the model results with moored measurements at the selected sites indicate fair agreement (Figure 5). The discrepancies are probably due to the existence of the diurnal amphidromic point and the resonant shelf wave. The model results at the SIB27 show great sensitivity to stratification, with less overestimation in summer. However, the present 3D model solutions show an improvement over *de Margerie and Lank*'s [1986] 2D model results in comparison with moored measurements over Banquereau Bank. The comparison also indicates a significant improvement over the solutions of the diagnostic model (the initial state of the prognostic model solutions; not shown).

3.3. Discussion

[25] The vertically integrated dissipation rates (illustrated by the spring solution in Figure 4c) indicate that dissipation associated with the tidal and seasonal-mean flows is partic-

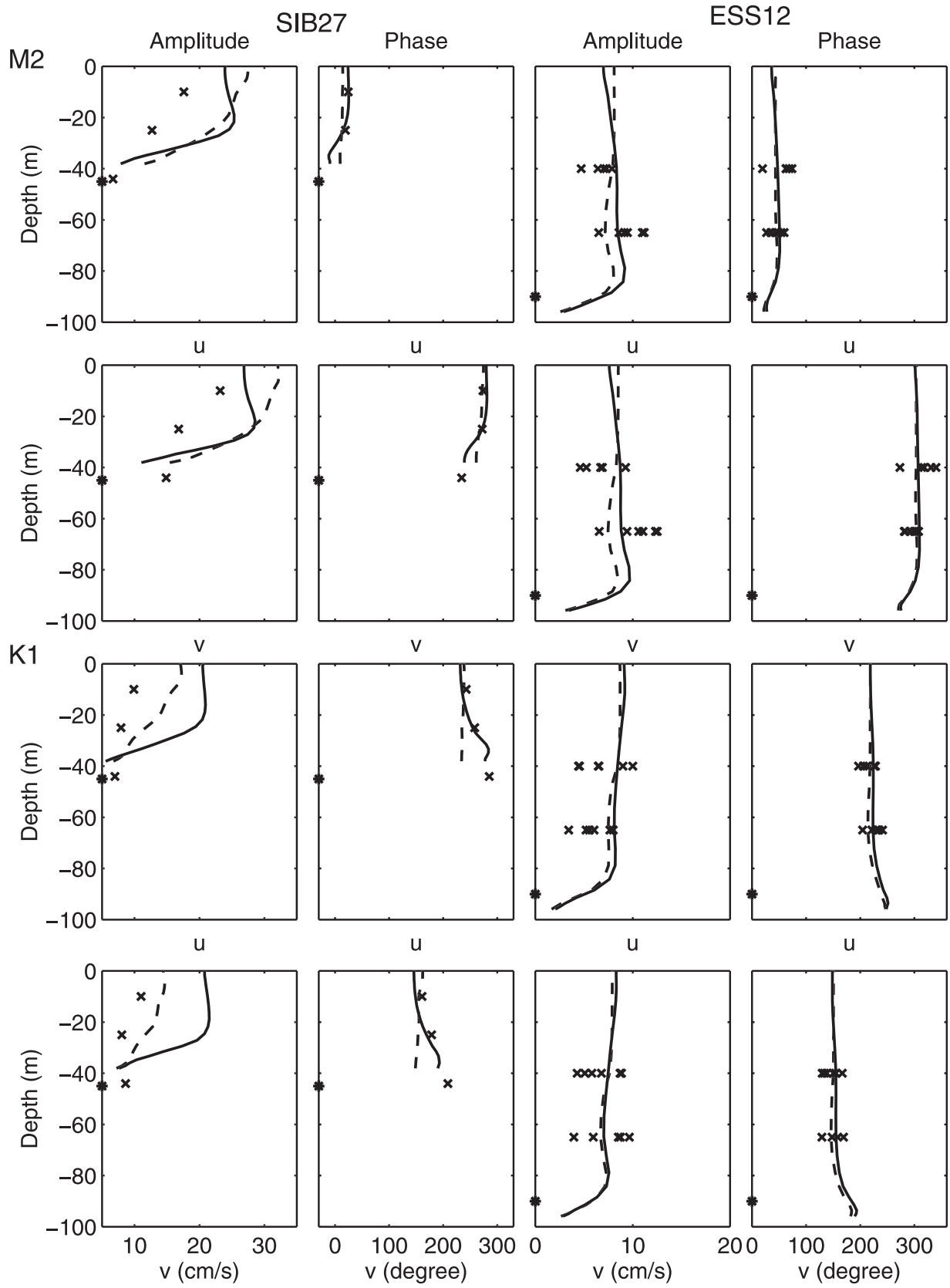

Figure 5. Computed vertical profiles and observed data for M_2 and K_1 currents (u and v are the eastward and northward components, respectively) at two selected sites SIB27 and ESS12. See Figure 4d for site locations. The model results are from the winter (solid line) and summer (dashed line) solutions. Observations were made at SIB27 in summer and at ESS12 in winter. The asterisk indicates the sounding depth.

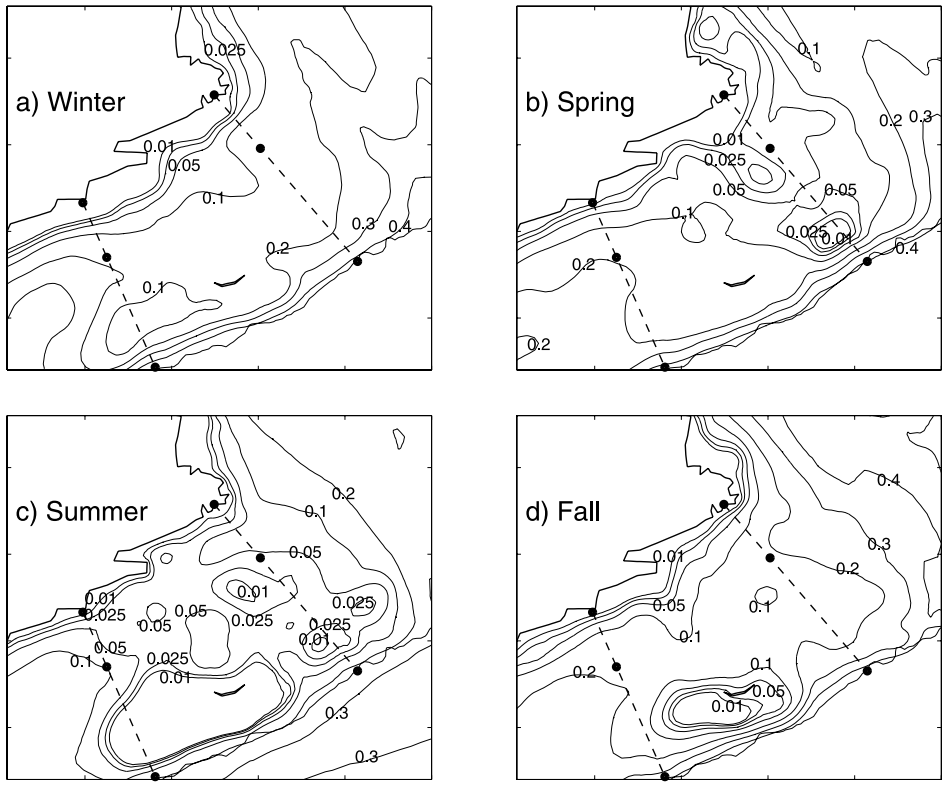

Figure 6. Transport stream function for the top 25 m in units of SV (10^6 m^3/s) for (a) winter, (b) spring, (c) summer, and (d) fall. The stream function value is zero along the Nova Scotia coast, with low values on the right looking downstream; that is, the flow is cyclonic around local stream function maxima and anticyclonic around local minima.

ularly significant over the shallow outer banks, with values generally in the range of 0.002–0.02 W/m^2. These values are comparable with measured values of (wind-forced) dissipation in the surface mixed layer on the Scotian Shelf in early fall [*Oakey and Elliott*, 1982], suggesting that tidal/mean-flow turbulence has substantial influences on the seasonal hydrodynamics over these banks through vertical mixing as well as through bottom stress. Since the tidal currents are generally larger than the mean flows in the solutions, most of the dissipation can be attributed to the tides. The dissipation rates over the banks are about 150% larger than those in *Hannah et al.*'s [2001] solutions owing to the inclusion of the K_1 tides here. Since the O_1 tide (not included here) is of comparable magnitude to the K_1 tide on the ESS [*Moody et al.*, 1984], the total tidal/mean-flow dissipation is probably underestimated by a similar percentage. We chose not to include the O_1 tide in the present study, since the resulting underestimation of dissipation may well be compensated for by the overestimation of the K_1 currents.

[26] Vertical stratification can suppress turbulence, reduce vertical mixing, and therefore affect tidal currents. At site ESS12, there are only minor differences between the winter and summer solutions (Figure 5), suggesting limited influences of the seasonal change in stratification (Figure 3). Larger seasonal changes can be seen in the model tidal currents at site SIB27, with the summer current amplitudes having enhanced vertical gradients above the bottom boundary layer due to the intensified stratification.

[27] The importance of friction to the tidal currents over the ESS is expected. For M_2, the barotropic pressure gradient is generally small over the ESS due to an in-phase co-oscillation with very limited spatial change in tidal elevation amplitude and phase, so the frictional effect in the momentum balance can be very important compared with the surface pressure gradient. For K_1, friction can be expected to have a significant influence on the location of the amphidromic point and on the resonance of the diurnal shelf wave.

[28] The evolution of density in the prognostic model should allow generation of baroclinic (internal) tides over varying bottom topography. There is observational evidence for internal tides in the Gully between Sable Island and Banquereau Banks [*Sandstrom and Elliott*, 1984], and in the moored current measurements (not shown). The present model output (Figure 3) indicates a diurnal displacement of the interior isopycnals (with a range of about 5 m), suggesting the existence of internal tides. However, an examination of the internal tides is beyond the scope of the present study and mesh. A higher-resolution model with better bottom topography is being used to further improve the barotropic tides and study baroclinic tides in the region.

4. Seasonal-Mean Circulation

[29] In this section, the prognostically refined seasonal-mean fields are described, interpreted, and compared with observations. The stream function for the vertically integrated transport in the upper 25-m layer (Figure 6) is used to present the near-surface circulation patterns, complemented by the velocity fields at 25-m depth (Figure 7). The vertical distributions of normal velocity and hydrographic properties

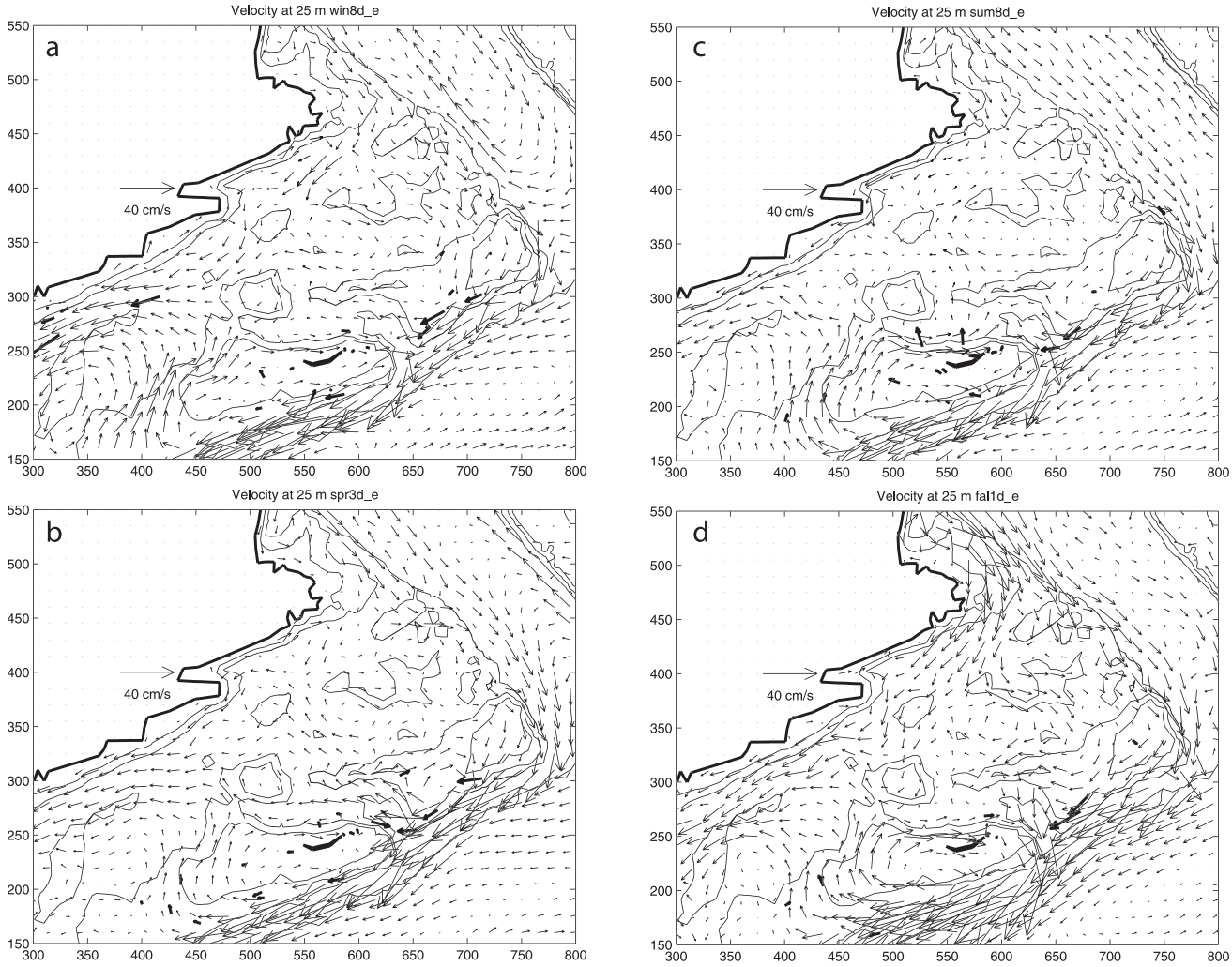

Figure 7. Model mean currents (thin arrows) at 25-m depth for (a) winter, (b) spring, (c) summer, and (d) fall from the prognostic model solutions. The model fields have been subsampled for clarity of presentation. The observed near-surface (10–20 m) currents (thick arrows) are also shown.

on selected sections (Figure 1), and the vertical profiles of current at selected observational sites (Figure 4d) are used to examine the 3D structure in particular areas of interest. Comparisons with observational transport estimates and moored current measurements are used to evaluate the flow fields.

[30] In all four seasons, the outflow from the Gulf of St. Lawrence through CS moves onto, or along the edge of, the ESS (Figures 6 and 7). Flow from the Newfoundland Shelf also contributes directly to circulation on the ESS, through crossovers across the outer Laurentian Channel and along the shelf edge. The primary shelf-scale flow features on the ESS are the shelf-break current which is an extension of the Labrador Current reinforced by a branch of the CS outflow [*Han et al.*, 1999], and the Nova Scotian Current (NSC) over the inner shelf which is initially supplied by a branch of the CS outflow and supplemented downstream by onshore meanders of the shelf-break flow [e.g., *Hannah et al.*, 2001].

4.1. CS Outflow and Bifurcation

[31] The outflow from the Gulf of St. Lawrence on the western side of CS has a strong influence on the hydrography and circulation over the ESS and its downstream coastal seas [e.g., *Hachey*, 1942; *Houghton and Fairbanks*, 2001]. It was long believed, based on water mass analysis and drift bottle studies, that a major portion of the outflow became the NSC flowing along the inner shelf, with the rest flowing along the western side of Laurentian Channel toward the Scotian Slope where mixing with the Labrador Current extension occurs. Recently, *Han et al.*'s [1999] diagnostic model solutions have indicated that the largest portion of the outflow moves offshore along the Channel's western side, and a smaller fraction flows along the inner shelf and onto the midshelf. Here we further examine the pathways of the CS outflow onto the ESS using the prognostically refined fields.

[32] The transport of the CS outflow in the prognostic solutions (Table 3) exhibits a significant seasonal variation, with a maximum of 1.3 Sv in fall and a minimum of 0.47 Sv in spring. The fall and summer values are close to *Han et al.*'s [1999] estimates, while the winter and spring transports are smaller than their values. The summer transport of 0.73 Sv is in good agreement with the

Table 3. Transports (in Sv) Across Key Sections in the Prognostically Refined Model Solutions With Wind, Baroclinic, Barotropic, and Tidal Forcing[a]

Period	CSW	B1	B2	L1	L2	H1	H2
Jan.–Feb.	0.71	0.22	0.9	0.34(0.6)	2.9	1.0(1.0)	1.75
April–May	0.5	−0.06	3.7	0.48	2.84	0.76	1.95
July–Aug.	0.73(0.84)	−0.09	1.8	0.23	1.78	0.5	0.22
Oct.–Nov.	1.27	0.30	1.8	0.45	0.83	0.75	2.48

[a]See Figure 1 for locations. Positive transports are southwestward, or seaward on the CSW. Observational estimates from *Anderson and Smith* [1989] and *Trites* [1972] are included in parentheses.

observational estimate of 0.84 Sv [*Trites*, 1972]. Section plots (Figures 8 and 9) indicate that the outflow in all seasons comprises surface-intensified jets mainly associated with the density gradients arising from the low-salinity water on the strait's western side (see Figure 8 of *Han et al.* [2002] for salinity plots corresponding to Figure 8). In all seasons the largest contributor to outflow transport is a jet over the entire water column between the 250- and 450-m isobaths. There is also a tendency in all seasons for a shallower outflow jet (upper 100 m or so) and flow reversal at depth closer to the Cape Breton coast (typically centered near the 200-m isobath), with the outflow jets appearing to be connected in three of the four seasons. Similar structures with different details, as well as weaker outflows further offshore, are present in the diagnostic initial fields and in the *Han et al.* [1999] solutions. Compared with the initial fields, the prognostic solutions have increased barotropic flows mainly located at the 300-m isobath, but the reliability of the detailed structure of the CS boundary flows is uncertain in view of the largely diagnostic approach used for the boundary conditions.

[33] East of Cape Breton Island, the CS outflow continues to move seaward over the shelf and on the western side of Laurentian Channel (Figures 6, 7, and 9). The flow offshore of the 200-m isobath in the channel is generally directed seaward year-round, except in winter when there is a suspect subsurface cyclonic cell in the outer channel [*Han et al.*, 1999]. The flow inshore of the 200-m isobath tends to turn westward around eastern Cape Breton Island, with distinct seasonal changes. In winter, summer, and fall, there are prominent flows hugging the Island's southeastern coast. The transport from CS directly onto the inner Scotian Shelf reaches its annual maximum in fall and winter, while in spring and summer, the CS outflow is weaker and mainly heads offshore along the western side of Laurentian Channel resulting in a weak transport onto the inner shelf (see next subsection). Overall, these solutions suggest that the flow from CS onto the ESS is more of a nearshore/shelf-edge bifurcation with more sluggish and confused flow on the midshelf, than the trifurcation suggested by *Han et al.* [1999]. The midshelf flow includes gyres and partial gyres but these do not appear to have a clear relation to topography, with the exception of the tendency for anticyclonic flow around Middle Bank associated principally with isotherms, isohalines, and isopycnals bowing downward over the bank (Figure 9).

[34] The nearshore flow off southeast Cape Breton is associated with the relatively fresh shallower CS outflow jet hugging the coast and turning right, presumably a tendency due to the Coriolis force [*Woods and Beardsley*, 1988]. However, the bulk of the transport in the deeper jet continues seaward along the western side of the channel, probably associated with vorticity constraints imposed by the shallow ESS topography. Thus the CS outflow bifurcation appears to be associated with differing influences of topography on the shallow inshore and deep offshore jets in the outflow. The flow across the Laurentian Channel from the southern Newfoundland Shelf (Figures 6 and 7) may also exert an influence on the pathway of the offshore-flowing branch [*Woods and Beardsley*, 1988].

4.2. Nova Scotian Current

[35] On the inner ESS the topography is complex, including an alongshore trench which is about 100–150 m deep and extends 50–100 km offshore of the coast connecting deep basins (>200 m) on the western side of the Laurentian Channel and off Halifax (Emerald Basin). Early drift bottle studies [e.g., *Trites and Banks*, 1958; *Bumpus and Lauzier*, 1965] indicated a continuous nearshore current, the NSC, along the shelf in spring and fall. Moored measurements of the NSC were made on the Halifax and Liscomb sections (Figure 1) and along the 100-m isobath between the two sections during the Canadian Atlantic Storms Program [*Anderson and Smith*, 1989]. Recent modeling investigations [*Han et al.*, 1997; *Hannah et al.*, 2001] have indicated that the NSC's core lies along the inshore trench on the ESS, and that it is intensified off Halifax by a branch of the shelf-break current that meanders to the inner shelf. However, there is presently limited quantitative knowledge about the NSC east of the Liscomb section.

[36] The present model results indicate that the NSC flows southwestward continuously near the surface (Figures 6 and 7), associated with isopycnal slopes primarily due to lower salinity over the inner shelf (Figures 10 and 11). There are significant seasonal variations in the peak speed, volume transport, location, and spatial extent of the NSC. Prominent alongshore variations in the transport magnitude (Table 3) and spatial extent (Figures 7, 10, and 11) are also evident. On the Banquereau section extending offshore from the eastern tip of Cape Breton (Figure 10), the salinity reaches a minimum in fall. There is no evidence of Slope Water at depth, with a typical two-layer temperature distribution in summer. The NSC's peak speed is about 25, 10, 10, and 15 cm/s in winter, spring, summer, and fall, respectively. In winter, the NSC is centered offshore of the 100-m isobath and separated from the Cape Breton coast by a countercurrent, and penetrates deeply over the entire water column. In summer, the NSC is closely attached to the Nova Scotia coast and confined to the upper 60 m, while in fall it is broader (about 70 km) than in the other seasons. The transport associated with the southwestward surface-intensified NSC at the Banquereau section changes seasonally from 0.5 Sv in fall and winter, to 0.1–0.15 Sv in spring and summer. However, because of the countercurrent, the net seasonal transports across the inner Banquereau section are 0.30, 0.22, −0.06, and −0.09 Sv in fall to summer, respectively (Table 3).

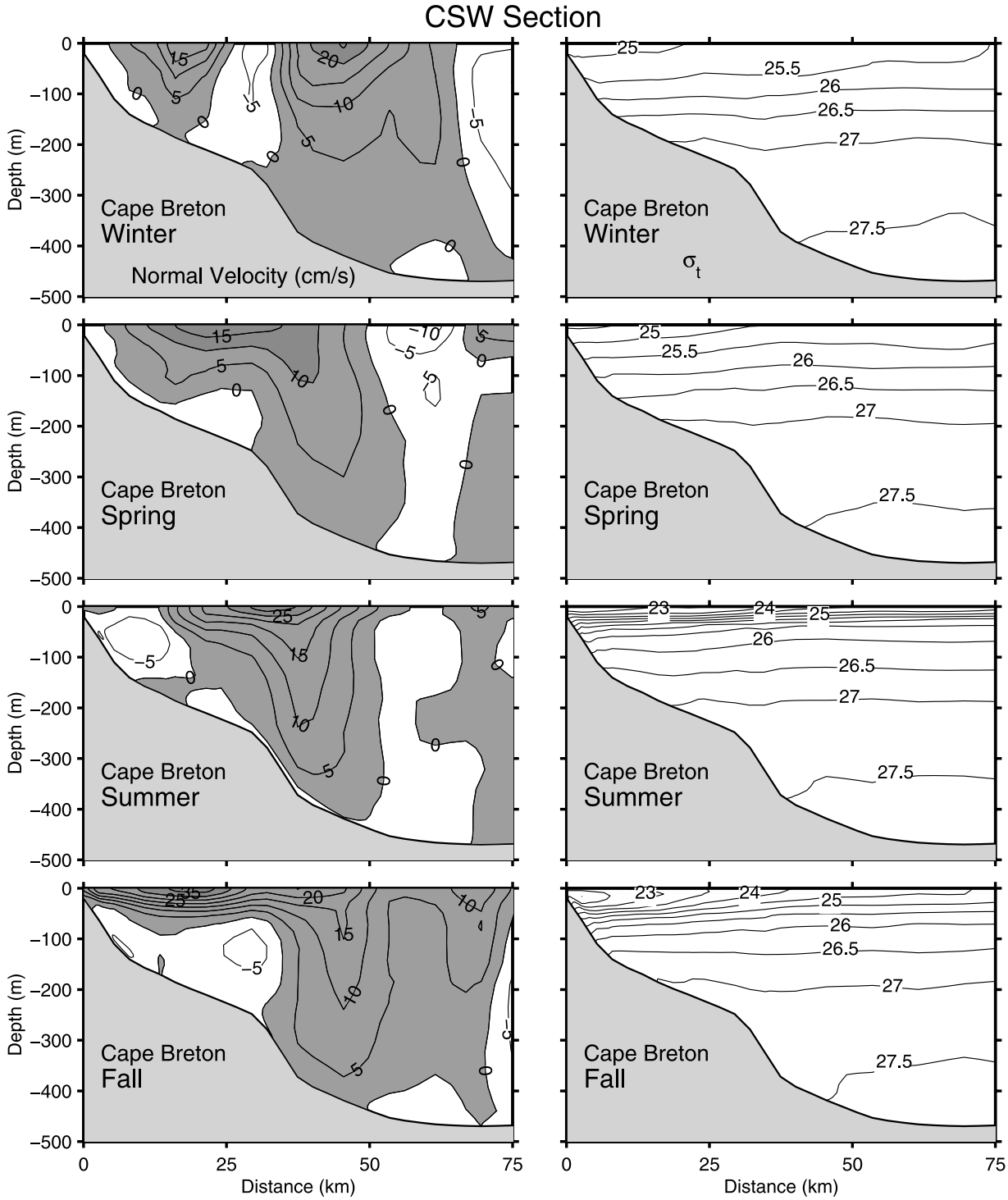

Figure 8. Mean normal velocity on the CSW section in winter, spring, summer, and fall from the model solutions. Also shown are the model density sections. The contour intervals are 5 cm/s for currents and 0.5 σ_t units for density. Positive values (shaded) indicate offshore currents.

[37] On the Liscomb section extending offshore across Sable Bank (Figure 11), intruded Slope Water at depth is evident, resulting in a three-layer temperature distribution in summer. The NSC is much broader (about 100 km) than on the Banquereau section in all the seasons, and extends much deeper in summer. The peak speed shows a similar seasonal cycle to that on the Banquereau section. The transport is largest in spring (0.53 Sv) and smallest in summer (0.23 Sv). Further downstream on the inner Halifax section the NSC transports are substantially larger, ranging from 0.5 Sv in summer to 1 Sv in winter (Table 3), as a result of the onshore meander west of Sable

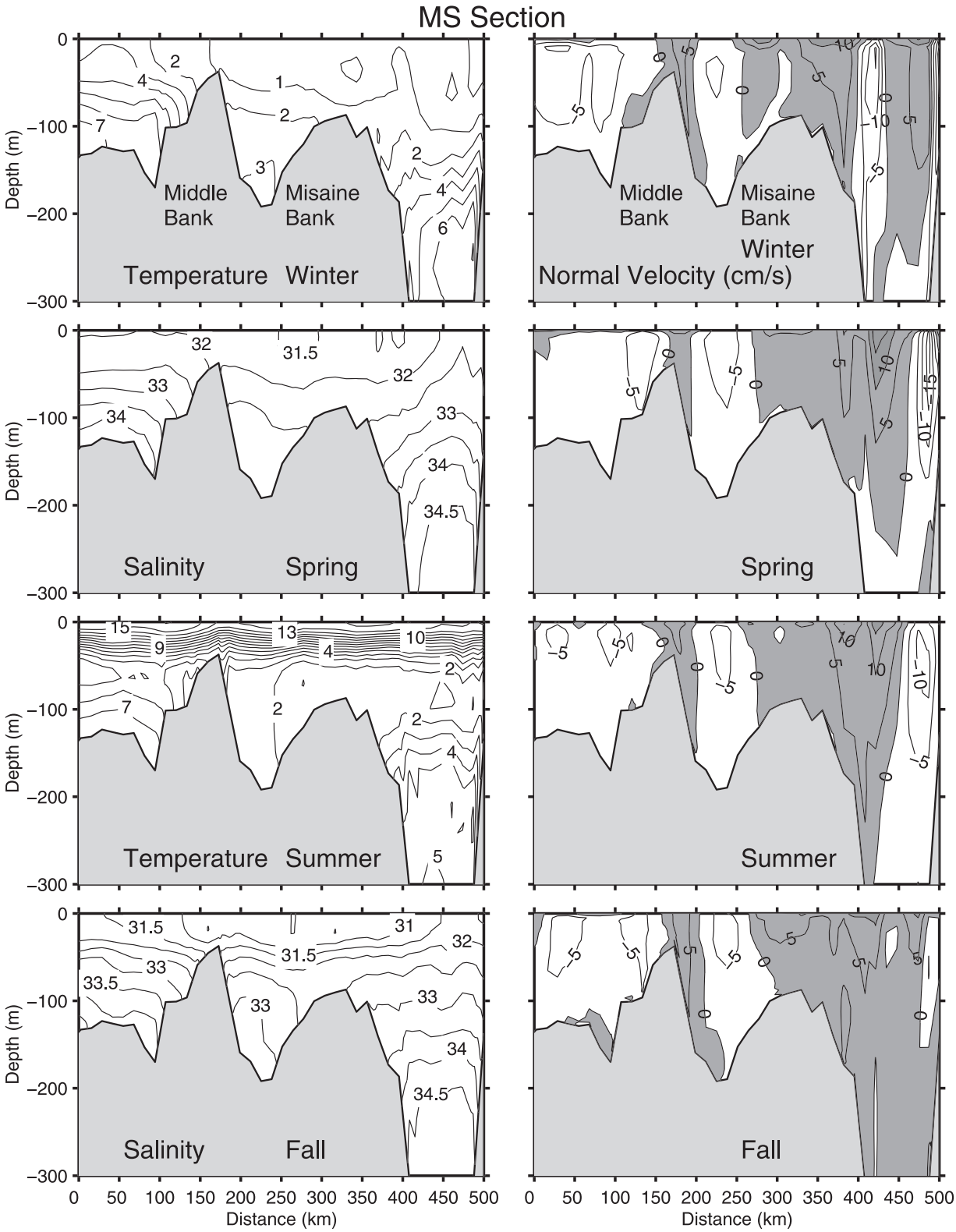

Figure 9. Vertical distribution of the model temperature (winter and summer) and salinity (spring and fall) on the MS section. Also shown are mean normal currents in the winter, spring, summer, and fall solutions. The contour intervals are 5 cm/s for currents, 1°C for temperature and 0.5 psu for salinity. Positive values (shaded) indicate offshore currents.

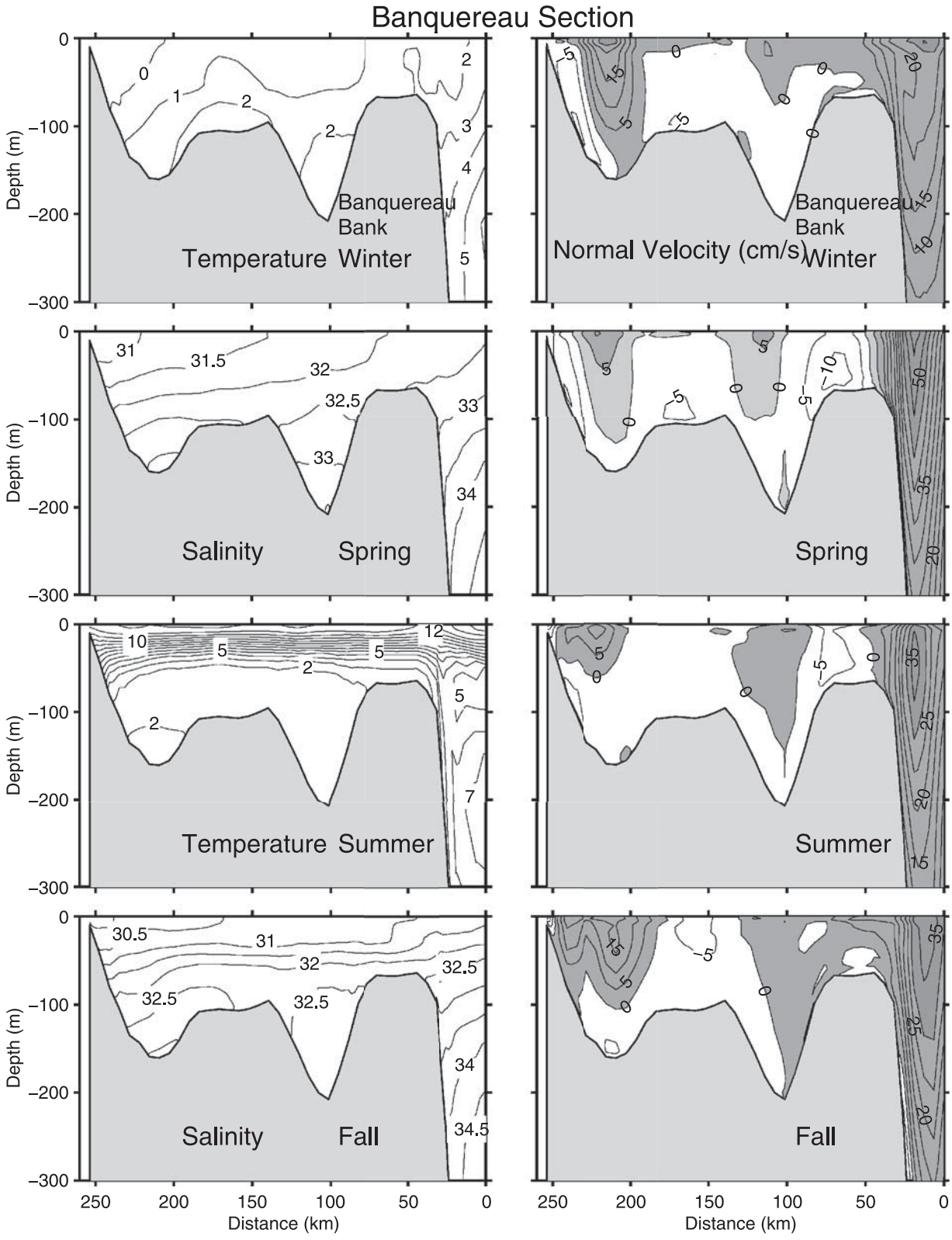

Figure 10. Vertical distribution of the model temperature (winter and summer) and salinity (spring and fall) on the Banquereau section. Also shown are mean normal currents in the winter, spring, summer, and fall solutions. The contour intervals are 5 cm/s for currents, 1°C for temperature, and 0.5 psu for salinity. Positive values (shaded) indicate southwestward currents.

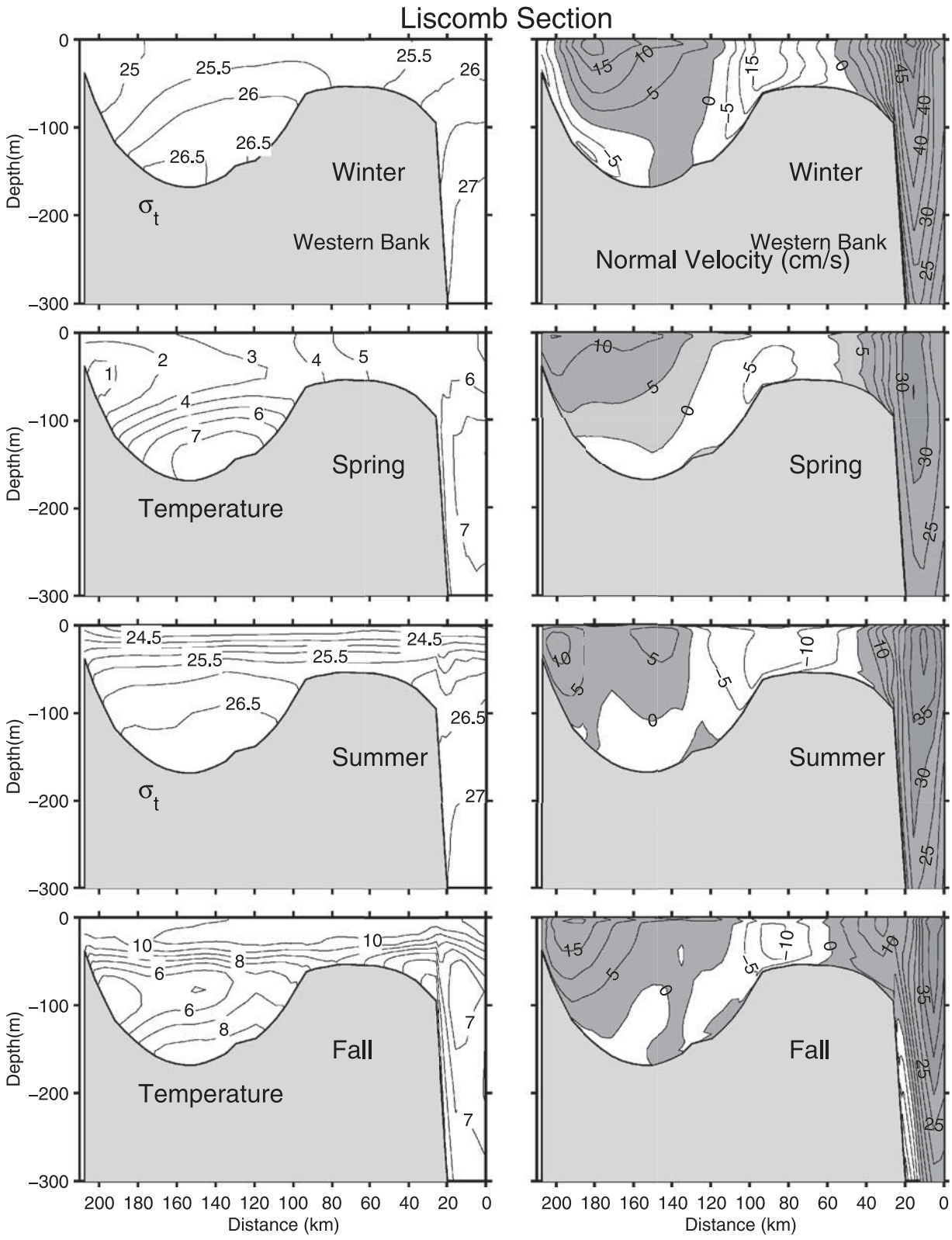

Figure 11. Vertical distribution of the model density (winter and summer) and temperature (spring and fall) on the Liscomb section. Also shown are mean normal currents in the winter, spring, summer, and fall solutions. The contour intervals are 5 cm/s for currents, 0.5 σ_t units for density, and 1°C for temperature. Positive values (shaded) indicate southwestward currents.

Bank of a branch of the shelf-break current [*Hannah et al.*, 2001] (Figure 7).

[38] A process partitioning study indicates that the NSC and its seasonal variation are primarily forced by baroclinic pressure gradients. The dominance of baroclinicity is also evident from the isopycnal slopes (Figure 11), and the strong vertical shears in the computed (Figures 10–12) and observed currents (Figure 12), mainly attributable to the low-salinity outflow from the Gulf of St. Lawrence. The contribution of the tidal rectification to the NSC is negligible during all seasons. The seasonal-mean current due to local wind-forcing is small compared to the speed of the southwestward NSC, except in summer when the former reduces the NSC's speed in the near-surface layer (within about 10 m of the surface). In essence, the NSC on the ESS is a nearshore branch of the CS outflow, and it is intensified on the central Scotian Shelf by onshore flow through the Gully in spring and through the Scotian Gulf and over Emerald and/or Western Banks in all seasons.

[39] Model transports across the inner part of the Halifax and Liscomb sections are in rough agreement with observational estimates in winter (Table 3). The current profiles (Figure 12) and the comparison statistics (Table 2) indicate that the model is in very good agreement with observations and reproduces both current magnitude and vertical shear in the NSC off Liscomb in winter.

4.3. Shelf-Break Current

[40] The shelf-break current is the largest coastal transport feature on the ESS. It is associated with the shelf/slope front, and includes contributions from the Gulf of St. Lawrence outflow via CS [e.g., *Han et al.*, 1999], the Labrador Current extension [e.g., *Smith and Schwing*, 1991; *Loder et al.*, 1998], and the northern branch of the cyclonic Slope Water gyre [*Csanady and Hamilton*, 1988]. The water mass structure in the front's vicinity has been discussed in the literature [e.g., *Gatien*, 1976; *Smith et al.*, 1978]. The shelf-break current and the nearshore NSC are important to climatic variability farther downstream in the northwest Atlantic's subpolar coastal current [*Chapman and Beardsley*, 1989]. However, unlike the NSC, there have been no direct current observations of the transport of the shelf-break current on the ESS.

[41] The prognostic model solutions (Figures 7, 10, and 11) show a surface-intensified shelf-break current that persists year-round, but has seasonal and alongshore variations in current magnitude and transport. On the Banquereau section (Figure 10), the peak currents are about 30 cm/s in winter, 35 cm/s in summer and fall, and 55 cm/s in spring. The transport across the outer Banquereau section (offshore to the 1000-m isobath) is also largest (3.7 Sv) in spring, smallest in winter (0.9 Sv), and intermediate in summer and fall (1.8 Sv) (Table 3). In contrast, the peak speed on the outer Liscomb section is largest in winter and smallest in spring, and the transport is largest (2.9 Sv) in winter and smallest (0.8 Sv) in fall. At the Halifax section, the shelf-break transport is as low as 0.2 Sv in summer, but substantially larger in fall (2.5 Sv), spring (2.0 Sv), and winter (1.8 Sv). The shelf-break current arises from baroclinic (vertical shear) and barotropic (bottom current) pressure gradients. These can have local artifacts and/or spatial shifts associated with aliased features in the initial density fields, so that some of the above seasonal and spatial differences may not be reliable. The present results together with those from previous studies [*Han et al.*, 1993, 1999; *Hannah et al.*, 2001] suggest that the shelf-break transport is largest in fall, winter, and spring, and substantially weaker in summer (the relatively low winter transport on the Banquereau section here appears to be associated with a suspicious density field feature in outer Laurentian Channel and a change in the Slope Water gyre of uncertain reliability). The alongshore transport decrease between the Banquereau and Liscomb sections in spring is partly associated with increased onshore flow through the Gully (section 4.5 and Figure 7). The significant reduction in the fall transport on the Liscomb section is due to an offshore shift of the shelf-break current and a near-bottom countercurrent reflecting a local anomaly in the baroclinic and/or barotropic pressure gradients.

[42] The present solutions indicate significant adjustment of the shelf-break current from its initial conditions (the diagnostic solutions). The shelf/slope front appears to be oversmoothed in the initial density fields (not shown) at depth. As a result, the diagnostic solutions based on these fields underestimate the associated shelf-break currents [also see *Han et al.*, 1997]. Enhanced isopycnal slopes at depth at the shelf edge in the prognostic model solutions (e.g., Figure 11) result in an intensified southwestward shelf-break current. The adjustment is mainly in the strength of the mean southwestward current associated with the mean density gradient. On the outer Liscomb section, the present prognostically refined model transports (2.9 Sv in winter and 1.8 Sv in summer) are close to *Han et al.*'s [1999] diagnostic estimates 3.1 and 2.2 Sv which included a considerable amount of barotropic inflow (1.8 Sv) on the SNS boundary in order to match observational transport estimates through CS. This suggests that the barotropic SNS inflow was overestimated in the *Han et al.* [1999] study because of the absence of prognostic dynamics [e.g., *Chapman and Lentz*, 1997].

4.4. Circulation Over Offshore Banks

[43] The topography of the outer ESS is dominated by a series of offshore banks along the shelf edge. Banquereau Bank is located on the eastern end of the ESS, and extends westward about 150 km from Laurentian Channel in the east to a large submarine canyon called the Gully. Then there are three banks in close proximity between the Gully and Scotian Gulf, with the shallowest Sable Bank in the east, Emerald Bank (minimum depth 65 m) in the west, and Western Bank (minimum depth 45 m) in between. There are several midshelf banks, most notably Misaine Bank inshore of Banquereau and Middle Bank connected to Sable Bank, and a variety of deep basins and channels between the banks.

[44] The model results indicate that the density structure varies from well-mixed areas over the outer banks' plateaus and weak surface-to-bottom fronts around the banks in winter, to moderate stratification in summer in the upper water column (Figures 9–11). Horizontal density gradients

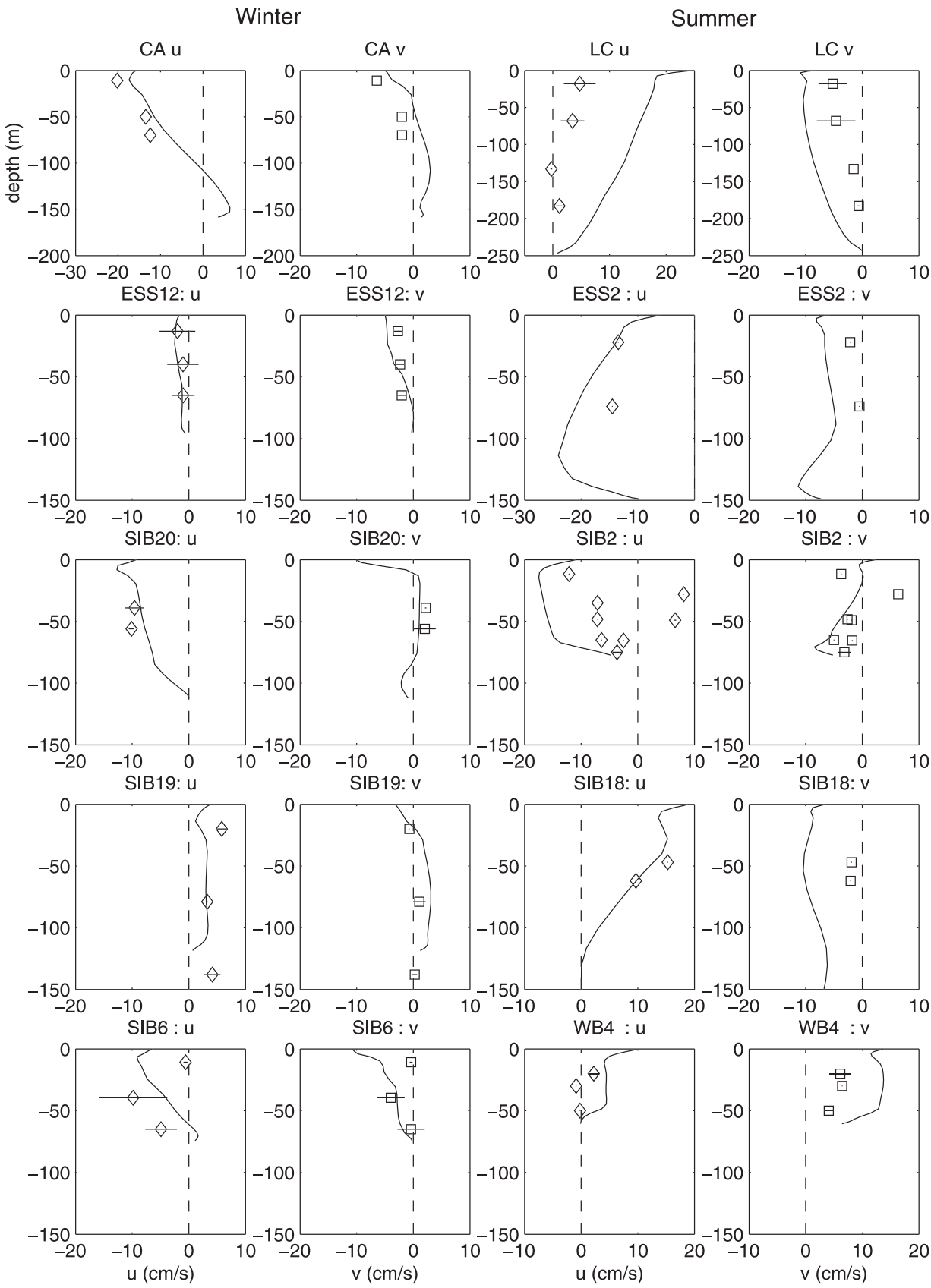

Figure 12. Comparison of model current profiles with observed bimonthly mean currents (open symbols) at selected sites and seasons. Here *u* and *v* are the eastward and northward components, respectively. The horizontal lines indicate the standard deviations of the individual observed monthly means about the bimonthly means. The site locations are shown in Figure 4d.

mainly occur at depth on the banks' sides (Figures 9 and 11), associated with a tendency for isopycnals in the lower water column to bow down over banks and up over basins. This results in a general tendency for surface-intensified baroclinic circulation in an anticyclonic sense over the banks and in a cyclonic sense over the intervening basins, similar to that found in other shallow seas with bank-basin topography [e.g., *Hill*, 1993]. This topographic-scale tendency can be seen (Figures 9 and 11) to be superimposed on the shelf-scale tendency for anticyclonic circulation on the ESS associated with the surface bowl of relatively fresh CS-outflow water extending from Laurentian Channel to Middle Bank.

[45] The model circulation over Banquereau Bank is typically a partial gyre with a strong offshore flow on its eastern side (western side of Laurentian Channel), the southwestward shelf-break current, and an onshore flow on its western side (eastern side of the Gully) (Figure 7). There are weak closed subgyres (5–10 cm/s) over the bank in spring and summer (see also Figures 6 and 10). An expanded southwestward shelf-break flow (15 cm/s) occupies most of the bank in fall. The offshore flow on the eastern side and the onshore flow on the western side are persistent features, but with prominent seasonal changes in their horizontal extent, core location, and magnitude.

[46] A broad anticyclonic gyre is the dominant feature inside the 100-m isobath over Sable, Western, and Emerald Banks in all seasons (Figure 7). The current magnitude in this gyre has a significant seasonal cycle: strongest in fall and weakest in spring. The transport in the fall gyre is 0.2–0.3 Sv. In winter, the gyre is centered over Western Bank, while in the other seasons it is generally centered on the western side of Sable Bank.

[47] The currents on the flanks of Western Bank (Figure 11) have significant surface intensification and extend over the entire water column in places, indicating both barotropic and baroclinic flow components [*Hannah et al.*, 2001]. In winter, there is strong onshore flow over the western end of Western Bank and over Emerald Bank. Near the surface, the wind-driven current reduces this onshore flow, but substantially reinforces the offshore flow on the eastern end of Sable Bank. In spring, the onshore flow is the weakest (5 cm/s) among all the seasons and mainly located on western Sable Bank, and the flow over Western Bank is very weak (less than 5 cm/s). In summer, there is onshore flow (15 cm/s) across Western Bank. In fall, the onshore flow is strongest with two branches: one on western Sable Bank, and the other on the western side of Western Bank with weaker circulation on the central Western Bank as indicated from in situ observations [e.g., *Griffin and Thompson*, 1996]. The anticyclonic gyres over the outer banks are strengthened by tidal rectification. Rectification of the M_2 and K_1 tides together contributes up to 5 cm/s to the along-bank current.

[48] Comparison with observational vertical current structure shows fair agreement (Figure 12). There is generally approximate agreement in direction and sign of the shear, but substantial differences in magnitude. It should be noted that, even at a particular site, the observations can be from different years so that temporal variability is aliased into apparent vertical structure in some cases (e.g., SIB2). The current comparison statistics (Table 1) indicate much better agreement in winter and fall than in spring and summer.

4.5. The Gully Partial Gyre

[49] The Gully is a large submarine canyon between Banquereau and Sable Banks, connecting the continental slope to the midshelf. In spite of increasing awareness of its uniqueness, biological significance, and ecological sensitivity [e.g., *Harrison and Fenton*, 1998], the Gully has not had a systematic current measurement program with moorings or drifters. The Gully may serve as a conduit of slope water to the inner shelf [*Houghton et al.*, 1978] through advection and mixing processes. A correlation analysis between temperature/salinity and currents [*Petrie et al.*, 1998] has indicated onshore-offshore exchange associated with low-frequency current fluctuations in the Gully. Recent modeling studies [*Han et al.*, 1997; *Hannah et al.*, 2001] have provided some knowledge about the Gully's seasonal circulation, but they were limited by either the simplified model dynamics and resolution, or proximity to the upstream open boundary.

[50] The present results indicate opposite overall horizontal density gradients across the Gully section between winter/spring and summer/fall (Figure 13), suggesting a net baroclinic transport onshore through the Gully in the former seasons and offshore in the latter seasons. The overall horizontal gradients are largest in spring, mainly associated with low-salinity water on the Banquereau side, resulting in a substantial (0.3–0.4 Sv) onshore transport. The gradients are significantly influenced by cold Labrador Slope Water at depth on the Banquereau side in summer and fall, resulting in a (slight) reversal in overall sign and reduced onshore transport. There is also a tendency for the isopycnals to turn down on the Gully (bank) sides associated with increased bottom boundary layer mixing, contributing to a year-round tendency for cyclonic circulation over the Gully. The computed circulation (Figures 7 and 13) indicates that another contributor to the cyclonic flow is onshore topographic steering of a branch of the shelf-break flow. However, a major portion of the southwestward shelf-break flow continues along the continental slope to the south, without an excursion into the Gully. There is a substantial seasonal variation in the current magnitude and structure of the partial cyclonic gyre, associated with the variations in the density field, shelf-break flow, and the Sable Bank gyre (whose northern/eastern branch contributes to the Gully partial gyre).

[51] The spring solution has a strong onshore flow through most of the Gully, and a weak offshore flow on the eastern side of the Gully (Figures 7 and 13). The onshore flow is steered through the Gully and along the western flank of Middle Bank toward the inner central shelf, strengthening the NSC. This onshore flow is an important advective mechanism for cross-shelf water exchange, and possibly for Slope Water intrusion in spring. This spring flow pattern is in significant contrast to the flow features around the Gully in the solutions for the other seasons. The spring peak of the onshore flow through the Gully is also different from the winter peak of the onshore flow on and to the western side of the Scotian Gulf. (It has been well recognized that the Scotian Gulf is the primary channel for Slope Water's intrusions into Emerald Basin.)

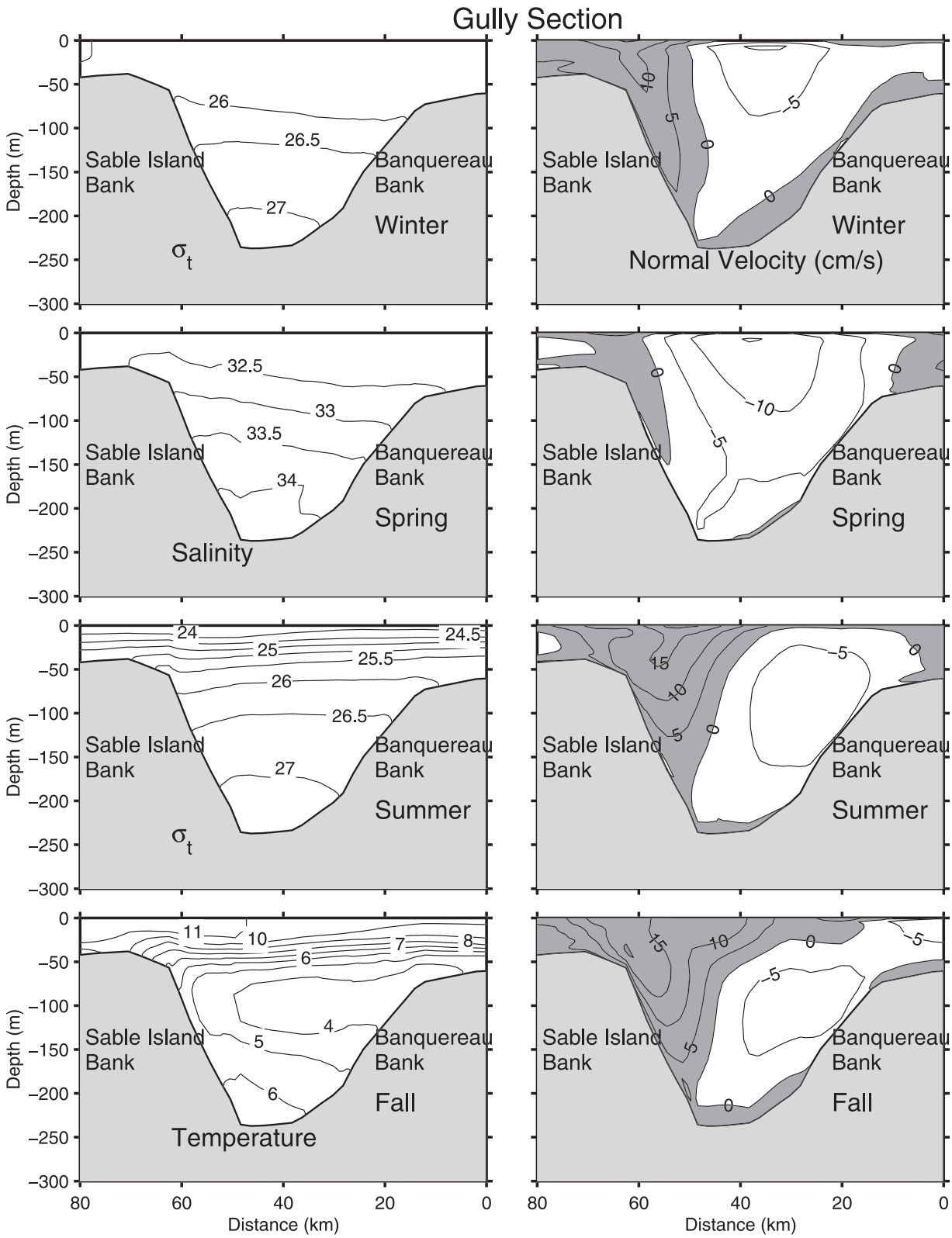

Figure 13. Vertical distribution of the model density (winter and summer), salinity (spring), and temperature (fall) on the Gully section. The contour intervals are 5 cm/s for currents, 0.5 σ_t units for density, 1°C for temperature, and 0.5 psu for salinity. Positive values (shaded) indicate offshore currents.

[52] Comparison with observed currents from the sides of Sable and Banquereau Banks shows good agreement in general (Figure 12). The model vertical current structure is consistent with the observed data. Observational data in the deep Gully are required to further validate model's ability of producing the Gully circulation.

5. Concluding Remarks

[53] The seasonal-mean circulation fields over the ESS from the prognostic model have indicated a strong and persistent shelf-break current and a more variable nearshore NSC, both flowing generally southwestward with substantial surface intensification. The fields show pronounced topographic-scale features over banks and basins, and substantial cross-shelf exchange.

[54] The prognostically refined flow fields provide a first quantitative and dynamically self-consistent description of the seasonal circulation implied by various ESS observational data sets. The circulation consists of flows from the Gulf of St. Lawrence (imposed at the CS boundary) and from the Newfoundland Shelf (imposed at the SNS boundary) with an overall southwestward flow tendency. The CS outflow onto the ESS occurs year-round as a seasonally varying bifurcation with branches onto the inner and outer shelf, and weaker and more variable flow onto the midshelf.

[55] The NSC in the model solutions is dominated by baroclinicity, and is in good agreement with available moored measurements. It has strong seasonal and alongshore variations in its transport and horizontal and vertical extents. The seasonal cycle of the volume transport of the model shelf-break current is qualitatively consistent with satellite altimeter observations [*Han et al.*, 1996] and diagnostic model solutions [*Han et al.*, 1997]. However, the prognostic solutions have stronger currents than the diagnostic ones because of sharpening of the shelf/slope front. The resulting current magnitudes are comparable with those in *Han et al.*'s [1999] solutions that were forced with additional barotropic boundary flows to give approximate agreement with observations in CS. The southwestward shelf-break (inside the 1000-m isobath) transport is typically in the range of 1–3 Sv (Table 3), with largest values generally in fall, winter, and spring, and on the more upstream (e.g., Banquereau) sections. The shelf-break flow includes baroclinic and barotropic components, and the solutions include some along-shelf variations apparently associated with local artifacts in the initial density fields.

[56] On topographic scales, the anticyclonic gyres or partial gyres over the outer banks, and the partial cyclonic gyre in the Gully are persistent features of the prognostically refined flow fields with significant seasonal variations. The model flows on the eastern Sable, Western, and Emerald Banks show prominent seasonal variability, including cross-shelf currents which contribute to the along-shelf changes of both the NSC and the shelf-break current.

[57] The inclusion of major tidal currents in the prognostic model provides a realistic representation of tidal friction and mixing effects in the model dynamics, and produces a first-cut representation of the 3D structure of the M_2 and K_1 tidal currents. The tidal solutions show approximate agreement with observational estimates, but there are notable discrepancies particularly for K_1. The latter appear to be related to a unique mixed tidal system over the ESS involving a resonant diurnal shelf wave, a nearby amphidrome, and substantial baroclinicity. These factors point to the need for improved model and topographic resolution in order to better simulate the system.

[58] The study results have indicated improved dynamical consistency of the prognostic model over the diagnostic model. The prognostic adjustment allows the model dynamics to filter out unphysical features in the initial temperature, salinity, density, and therefore circulation fields, and to restore robust features that may have been oversmoothed in the diagnostic solutions. In particular, the regional prognostic model reduces the need for the inclusion of artificial barotropic inflows to compensate for oversmoothed interior density fields and underestimated baroclinic currents in diagnostic solutions [e.g., *Han et al.*, 1999]. Nevertheless, moored measurements in key locations of the open boundary, nested modeling, and/or data assimilation are needed for improving open boundary conditions, particularly on the southern Newfoundland Shelf and at CS.

[59] **Acknowledgments.** We wish to thank Shawn Oakey for assistance with the postprocessing of model results, Dan Lynch and Chris Naimie for providing the numerical models, Dave Greenberg and Charles Hannah for contributions to model implementation, and the many contributors to the historical observational data sets for the region. Jim Helbig and Don Lawrence provided useful internal reviews. Useful comments were received from an anonymous reviewer. This work has been funded through the Offshore Environmental Factors program of the (Canadian) Program for Energy Research and Development, and through the Gully studies program of Fisheries and Oceans Canada.

References

Anderson, C., and P. C. Smith, Oceanographic observations on the Scotian Shelf during CASP, *Atmos. Ocean*, *27*, 130–156, 1989.

Blumberg, A. F., B. Galperin, and D. J. O'Connor, Modeling vertical structure of open-channel flows, *J. Hydraul. Eng.*, *118*, 1119–1134, 1992.

Brander, K., and P. C. F. Hurley, Distribution of early-stage Atlantic cod (*Gadus morhua*), haddock (*Melanogrammus aeglefinus*), and witch flounder (*Glyptocephalus cynoglossus*) eggs on the Scotian Shelf: A reappraisal of evidence on the coupling of cod spawning and plankton production, *Can. J. Fish. Aquat. Sci.*, *49*, 238–251, 1992.

Bumpus, D. F., and L. M. Lauzier, Surface circulation on the continental shelf of eastern North America between Newfoundland and Florida, in *Serial Atlas of the Marine Environment*, folio 7, Plate 8, 4 pp., Am. Geogr. Soc., New York, 1965.

Chapman, D. C., and R. C. Beardsley, On the origin of shelf water in the Middle Atlantic Bight, *J. Phys. Oceanogr.*, *19*, 384–391, 1989.

Chapman, D. C., and S. J. Lentz, Adjustment of stratified flow over a sloping bottom, *J. Phys. Oceanogr.*, *27*, 340–356, 1997.

Csanady, G. T., and P. Hamilton, Circulation of slopewater, *Cont. Shelf Res.*, *8*, 565–624, 1988.

de Margerie, S., and K. D. Lank, Tidal circulation of the Scotian Shelf and Grand Bank, *Rep. FD901-5-X515*, Dep. of Fish. and Oceans Can., Vancouver, B. C., Can., 1986.

Foreman, M. G. G., R. E. Thomson, and C. L. Smith, Seasonal current simulations for the western continental margin off Vancouver Island, *J. Geophys. Res.*, *105*, 19,665–19,668, 2000.

Frank, K. T., J. E. Carscadden, and J. E. Simon, Recent excursions of capelin (*Mallotus villosus*) to the Scotian Shelf and Flemish Cap during anomalous hydrographic conditions, *Can. J. Fish. Aquat. Sci.*, *53*, 1473–1486, 1996.

Gatien, M. G., A study in the slope water region south of Halifax, *J. Fish. Res. Board Can.*, *33*, 2213–2217, 1976.

Gordon, D. C., L. D. Griffiths, G. V. Hurley, A. L. Muecke, D. K. Muschenheim, and P. G. Wells (Eds.), Understanding the environmental effects of offshore hydrocarbon development, Proceedings of a workshop, *Can. Tech. Rep. Fish. Aquat. Sci.*, *2311*, 116 pp., 2000.

Gregory, D. N., and C. Bussard, Current statistics for the Scotian Shelf and Slope, in *Can. Data Rep. Hydrogr. Ocean Sci.*, *144*, 167 pp., 1996.

Griffin, D. A., and K. R. Thompson, The adjoint method of data assimilation used operationally for shelf circulation, *J. Geophys. Res.*, *101*, 3457–3477, 1996.

Hachey, H. B., The waters of the Scotian Shelf, *J. Fish. Res. Board Can.*, *5*, 377–397, 1942.

Han, G., Three-dimensional modeling of tidal currents and mixing quantities over the Newfoundland Shelf, *J. Geophys. Res.*, *105*, 11,407–11,422, 2000.

Han, G., M. Ikeda, and P. C. Smith, Annual variation of sea-surface slopes over the Scotian Shelf and Grand Banks from Geosat altimetry, *Atmos. Ocean*, *31*, 591–615, 1993.

Han, G., M. Ikeda, and P. C. Smith, Oceanic tides over the Newfoundland and Scotian Shelves from TOPEX/POSEIDON altimetry, *Atmos. Ocean*, *34*, 589–604, 1996.

Han, G., C. G. Hannah, J. W. Loder, and P. C. Smith, Seasonal variation of the three-dimensional mean circulation over the Scotian Shelf, *J. Geophys. Res.*, *102*, 1011–1025, 1997.

Han, G., J. W. Loder, and P. C. Smith, Seasonal-mean hydrography and circulation in the Gulf of St. Lawrence and eastern Scotian and southern Newfoundland Shelves, *J. Phys. Oceanogr.*, *29*, 1279–1301, 1999.

Han, G., C. L. Tang, and P. C. Smith, Annual variations of sea surface elevations and currents over the Scotian Shelf and Slope, *J. Phys. Oceanogr.*, *32*, 1794–1810, 2002.

Hannah, C. G., J. W. Loder, and D. G. Wright, Seasonal variation of baroclinic circulation in the Scotia-Maine region, in *Boundary Effects on Coastal Dynamics, Coastal Estuarine Stud.*, vol. 53, edited by D. G. Aubrey and C. T. Friedichs, pp. 7–29, AGU, Washington, D. C., 1996.

Hannah, C. G., J. Shore, J. W. Loder, and C. Naimie, Seasonal circulation on western and central Scotian Shelf, *J. Phys. Oceanogr.*, *31*, 591–615, 2001.

Harrison, W. G., and D. G. Fenton, The Gully: A scientific review of its environment and ecosystem, *Res. Doc. 98/83*, 282 pp., Can. Stock Assess. Secretariat, Ottawa, 1998.

Head, E. J. H., L. R. Harris, and B. Petrie, Distribution of *Calanus* spp. on and around the Nova Scotia Shelf in April: Evidence for an off-shelf source of *Calanus finmarchicus* to the central and western regions, *Can. J. Fish. Aquat. Sci.*, *56*, 2476–2663, 1999.

Herman, A. W., D. D. Sameoto, C. Shunnian, M. R. Mitchell, B. Petrie, and N. Cochrane, Sources of zooplankton on the Nova Scotia Shelf and other aggregations within the deep shelf basins, *Cont. Shelf Res.*, *11*, 211–238, 1991.

Hill, A. E., Seasonal gyres in shelf seas, *Ann. Geophys.*, *11*, 1130–1137, 1993.

Houghton, R. W., and R. G. Fairbanks, Water sources for Georges Bank, *Deep Sea Res., Part II*, *48*, 95–114, 2001.

Houghton, R., P. C. Smith, and R. O. Fournier, A simple model for cross-shelf mixing on the Scotian Shelf, *J. Fish. Res. Board Can.*, *35*, 414–421, 1978.

Loder, J. W., G. Han, C. G. Hannah, D. A. Greenberg, and P. C. Smith, Hydrography and baroclinic circulation in the Scotian Shelf region: Winter vs. summer, *Can. J. Fish. Aquat. Sci.*, *54*, Suppl. 1, 40–56, 1997.

Loder, J. W., B. D. Petrie, and G. Gawarkiewicz, The coastal ocean off northeastern North America: A large-scale view, in *The Global Coastal Ocean: Regional Studies and Synthesis*, vol. 11, *The Sea*, edited by K. H. Brink and A. R. Robinson, chap. 5, pp. 105–133, John Wiley, New York, 1998.

Lynch, D. R., J. T. C. Ip, C. E. Naimie, and F. E. Werner, Comprehensive coastal circulation model with application to the Gulf of Maine, *Cont. Shelf Res.*, *16*, 875–906, 1996.

McLellan, H. J., Bottom temperature on the Scotian Shelf, *J. Fish. Res. Board Can.*, *11*, 404–418, 1954.

Mellor, G. L., and T. Yamada, Development of a turbulence closure model for geophysical fluid problems, *Rev. Geophys.*, *20*, 851–875, 1982.

Moody, J. A., et al., Atlas of tidal elevation and current observations on the Northeast American Continental Shelf and slope, *U.S. Geol. Surv. Bull.*, *1611*, 122, 1984.

Naimie, C. E., Georges Bank residual circulation during weak and strong stratification periods: Prognostic numerical model results, *J. Geophys. Res.*, *101*, 6469–6486, 1996.

Naimie, C. E., and D. R. Lynch, *FUNDY5 Users' Manual*, 40 pp., Numer. Method. Lab., Dartmouth Coll., Hanover, N. H., 1993.

Oakey, N. S., and J. A. Elliott, Dissipation within the surface mixed layer, *J. Phys. Oceanogr.*, *12*, 171–185, 1982.

Page, F. H., and R. J. Losier, Temperature variability during Canadian bottom-trawl summer surveys conducted in NAFO Division 4VWX, 1970–1992, *ICES Mar. Sci. Symp.*, *198*, 323–331, 1994.

Petrie, B., and P. A. Yeats, Annual and interannual variability of nutrients in the Scotian Shelf-Gulf of Maine region, *Can. J. Fish. Aquat. Sci.*, *57*, 2536–2546, 2000.

Petrie, B., K. Drinkwater, D. Gregory, R. Pettipas, and A. Sandstrom, Temperature and salinity atlas for the Scotian Shelf and Gulf of Maine, *Can. Tech. Rep. Hydrogr. Ocean Sci. 171*, 398 pp., Dep. Of Fish. and Oceans, Inst. of Ocean Sci., Sidney, B. C., Can., 1996.

Petrie, B., J. Shore, C. Hannah, and J. Loder, Physical oceanography, in The Gully: A scientific review of its environment and ecosystem, edited by W. G. Harrison and D. G. Fenton, *Can. Stock Assess. Secr. Res. Doc. 98/83*, pp. 20–57, Mar. Reg. Adv. Process Dep. of Fish. and Oceans, Dartmouth, N. S., Can., 1998.

Sandstrom, H., and J. Elliott, Internal tide and solitons on the Scotian Shelf: A nutrient pump at work, *J. Geophys. Res.*, *89*, 6415–6426, 1984.

Sheng, J., and K. Thompson, Summer surface circulation on the Newfoundland Shelf and Grand Banks: The roles of local density gradients and remote forcing, *Atmos. Ocean*, *43*, 257–284, 1996.

Smith, P. C., and B. D. Schwing, Mean circulation and variability on the eastern Canadian continental shelf, *Cont. Shelf Res.*, *11*, 977–1012, 1991.

Smith, P. C., B. Petrie, and C. R. Mann, Circulation, variability and dynamics of the Scotian Shelf and Slope, *J. Fish. Res. Board Can.*, *35*, 1067–1083, 1978.

Smith, P. C., R. W. Houghton, R. G. Fairbanks, and D. G. Mountain, Interannual variability of boundary fluxes and water mass properties in the Gulf of Maine and on Georges Bank: 1993–1997, *Deep Sea Res., Part II*, *48*, 37–70, 2001.

Taggart, C. T., K. R. Thompson, G. L. Maillet, S. E. Lochmann, and D. A. Griffin, Abundance distribution of larval cod (*Gadus morhua*) and zooplankton in a gyre-like water mass on the Scotian Shelf, in *Survival Strategies in Early Life Stages of Marine Resources*, edited by Y. T. Watanabe and Y. Oozecki, pp. 155–173, A. A. Balkema, Brookfield, Vt., 1996.

Thompson, K. R., and D. A. Griffin, A model of the circulation on the outer Scotian Shelf with open boundary conditions inferred by data assimilation, *J. Geophys. Res.*, *103*, 30,641–30,660, 1998.

Trites, R. W., The Gulf of St. Lawrence from a pollution point of view, in *Marine Pollution and Sea Life*, edited by M. Ruivo, pp. 59–72, Fishing News Books, London, 1972.

Trites, R. W., and R. E. Banks, Circulation on the Scotian Shelf as indicated by drift bottles, *J. Fish. Res. Board Can.*, *15*, 79–89, 1958.

Woods, A. W., and R. C. Beardsley, On the barotropic discharge of a homogeneous fluid onto a continental shelf, *Cont. Shelf Res.*, *8*, 307–327, 1988.

G. Han, Biological and Physical Oceanography Section, Fisheries and Oceans Canada, Northwest Atlantic Fisheries Centre, P.O. Box 5667, St. John's, NewFoundland, Canada A1C 5X1. (hang@dfo-mpo.gc.ca)

J. W. Loder, Ocean Sciences Division, Fisheries and Oceans Canada, Bedford Institute of Oceanography, Dartmouth, Nova Scotia, Canada B2Y 4A2. (loderj@mar.dfo-mpo.gc.ca)